

**KERNFORSCHUNGSZENTRUM  
KARLSRUHE**

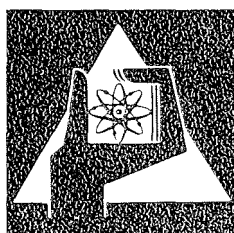
August 1976

KFK 2330

Institut für Angewandte Kernphysik

**Nuclear Matter Distribution from Scattering of Strongly  
Interacting Projectiles**

H. Rebel



**GESELLSCHAFT  
FÜR  
KERNFORSCHUNG M.B.H.**

**KARLSRUHE**

Als Manuskript vervielfältigt

Für diesen Bericht behalten wir uns alle Rechte vor

GESELLSCHAFT FÜR KERNFORSCHUNG M. B. H.  
KARLSRUHE

KERNFORSCHUNGSZENTRUM KARLSRUHE

KFK 2330

Institut für Angewandte Kernphysik

NUCLEAR MATTER DISTRIBUTION FROM SCATTERING  
OF STRONGLY INTERACTING PROJECTILES

Heinigerd Rebel

Gesellschaft für Kernforschung m.b.H., Karlsruhe

Invited Lectures presented at the Second Conference  
"Radial Shape of Nuclei", Cracow, Poland, June, 22-25, 1976



## Abstract

Nucleon and  $\alpha$ -particle scattering has been reviewed with the aspect of the information on the nuclear matter distribution, in particular at the surface, and on size and shape of nuclei.

Die Verteilung der nuklearen Materie in Kernen gewonnen aus der Streuung starkwechselwirkender Projektile

## Zusammenfassung

Die Streuung von Nukleonen und  $\alpha$ -Teilchen wird hinsichtlich ihrer Information über die Verteilung der nuklearen Materie an der Kernoberfläche sowie über Größe und Gestalt der Atomkerne diskutiert.

Zum Druck eingereicht am 15.6.1976

## 1. INTRODUCTION

The nuclear matter distribution can be investigated only through phenomena involving the nuclear interaction. Since this is not nearly so well understood as the Coulomb interaction, our knowledge of the nuclear matter distribution is much less precise than that of the nuclear charge distribution. Many methods have been proposed and applied to study the nuclear matter distribution. They all have considerable difficulties and uncertainties. But to the extent that they lead to consistent results the knowledge obtained from them all is greater and more convincing than that from each in isolation. Tab. 1 compiles several methods and indicates some typical examples of the basic concepts. The methods cover a tremendous energy range of the used probes, and also a tremendous range of type of probe: proton, neutron,  $\alpha$ -particle, photon, pion, K-meson and antiproton. Part of these methods reveals primarily the total nuclear matter distribution, and using the charge distribution obtained from electron scattering e.g., information about the neutron distribution may be extracted. Some experiments are based on specific effects which depend on the neutron-proton ratios in the outermost region of the nucleus and primarily highlight differences in the spatial distributions  $\rho_n$  and  $\rho_p$  at the nuclear surface.

In the present report we are mainly concerned with the scattering of strongly interacting projectiles which seems to be a widely used standard method of studying nuclear matter distributions. Thereby the reliability of the information found is intimately connected with our understanding of the optical potential in terms of the spatial distribution of the nucleons in nuclei.

The optical model is of central importance for interaction processes of nuclear particles, and for many years now it has been a standard procedure to interpret scattering experiments in terms of an average complex potential the shape of which because of the short range of the nuclear forces is assumed to be of the same general form as that of the nuclear density distribution. Numerous analyses of scattering cross sections, angular distributions and polarization data have established the gross features and details

Experimental methods of studying nuclear matter distributions

	Illustrative Examples - Concept -	Reference
<u>Nucleon scattering</u>	30 MeV p scattering (ROM) 1 GeV p scattering	Green 68-70 Thir 74 - Ahm 75
<u>Scattering of strongly absorbed projectiles:</u> $\tau, \alpha, {}^{16}\text{O}$	${}^{40,48}\text{Ca}(\alpha, \alpha)$ (ROM) at $E_\alpha = 79\text{MeV}$ ${}^{204,206,208}\text{Pb}(\alpha, \alpha)$ (ROM) at $E_\alpha = 104\text{MeV}$ ${}^{116-124}\text{Sn}(\alpha, \alpha)$ ${}^{116-124}\text{Sn}({}^{16}\text{O}, {}^{16}\text{O})$ at E near the Coulomb barrier	Lern 75 Gi Re 76 Tab 75
Total and reaction cross sections: $p, \bar{p}, n, \pi, K$ Absorption of $\pi^\pm$ Coherent photo production of neutral mesons $\pi$ production Photo nuclear processes Charge exchange with $\pi$ and K	1.5-30 GeV/c n scattering 20-60 GeV/c $\pi$ scattering 0.7-2.0 GeV/c $\sigma_R(\pi^-) / \sigma_R(\pi^+)$ ratios ( $\gamma, \pi^0$ ) ( $\gamma, g^0$ ) $\pi^+/\pi^-$ production ratio with 600 MeV protons by ${}^{12}\text{C}$ and ${}^{208}\text{Pb}$ ( $\gamma, xn$ ) $\pi^\pm(K^\pm) + A(Z, N) \rightleftharpoons$ $\pi^0(K^0/\bar{K}^0) + A(Z\pm 1, N\mp 1)$	Fran 72 Bat Fri 72 Alla 73 Leis 58 Alv 70 { Marg 68 Tann 69 Leo 73 Ko Ma 69 (proposed)
(p,n) quasi elast. reaction Coulomb displace- ment energies $\alpha$ - decay $\beta$ - decay	${}^{208}\text{Pb}(p, n) {}^{208}\text{Bi}$ IAS Neutron excess radii interpretation decay rate dependence of barrier height and position ft values of super - allowed transitions - hgh. order corrections	Fri 74 No Sch 69 Rho Ja 76 Bli 69
Hadronic atoms	K - capture $\bar{p}$ - capture	Le Se 74 Bug 73

Tab. 1

of the phenomenological forms of the optical potentials specified by empirical sets of parameters describing strength, radial size and deformation (but usually suffering from some ambiguities since the interior parts of the potentials play a minor role and are less determined by the scattering data).

However, the traditional, highly phenomenological interpretation does not provide deeper insight into more microscopic aspects of the reaction mechanism. From microscopic point of view we seek to describe the scattering of the projectile from a nucleus on the basis of more fundamental interactions starting from the nucleon-nucleon force in terms of motions of individual nucleons. In all aspects this is a very ambitious project. But even if we transform the original problem into a problem of particles via an "effective interaction" and are satisfied with phenomenological descriptions of size and shape of the nucleus and in particular of its collective modes, the macroscopic optical model basis is rather insufficient as it represents already a convolution of properties of the target nucleus and the probing projectile. Primarily the size and deformation parameters extracted by the traditional analysis characterize the *interaction potential*, and the information about more fundamental quantities characterising the nuclear density distribution remains rather indirect and unclear. Thus, if we are interested in properties of the nuclear density distribution, it is obviously more reasonable to formulate the scattering model in terms of the matter or nucleonic distribution. Several microscopic models which construct the optical potential from the nucleonic density distribution and an adequate projectile - bound nucleon interaction have been worked out: Kerman-McManus-Thaler (KMT) approach [Ker 59, Fes Hü 70, Fes 71], Greenlees (ROM) approach [Green 68-70], and their later improvements, refinements and extensions.

In the framework of a multiple scattering theory [Wat 53] the optical potential is given by a multiple scattering series

$$U = \langle 0 | \sum_j t_j | 0 \rangle + \langle 0 | \sum_{j \neq k} t_j Q G_o t_k | 0 \rangle + \dots \quad (1.1)$$

where the projectile - bound nucleon operator  $t_j$  is defined by

$$t_j = v_j + v_j Q G_o t_j \quad (1.2)$$

and the projectile-nucleus interaction  $V$  is assumed to be a sum of two-body interactions  $v_j(\vec{r}_j, \vec{r}_p)$  with each target nucleon. The operator  $Q$  projects off the groundstate of the target nucleus and  $G_0$  is the propagator

$$G_0^\pm = (E - H_N - h_p - K_p \pm i\eta) \quad (1.3)$$

with the nuclear Hamiltonian  $H_N$ , the internal Hamiltonian  $h_p$  of the projectile and the kinetic energy operator  $K_p$ . The energy of the system  $E = E_{kin} + \epsilon_N$  is the kinetic energy and the excitation energy, usually of the nucleus alone (even when applying the approach to complex projectiles). The first term of the expansion represents single scattering summed to all orders and averaged over all the nucleons in the nucleus. The higher order terms describing successive single scattering from different nucleons involve in intermediate states nuclear excitation.

The exact scattering amplitude is given by

$$f(\vec{k}, \vec{k}') = \langle \vec{k} | U + U G_0 U + \dots | \vec{k}' \rangle \quad (1.4)$$

Taking the first term in each expansion we obtain the Born approximation with the scattering amplitude proportional to nuclear formfactor

$$F_m(q) = \int e^{i\vec{q}\vec{r}} \rho_m(r) dr \quad (\vec{q} = \vec{k} - \vec{k}') \quad (1.5)$$

which is a Fourier transform of the nuclear matter distribution  $\rho_m$ . Born approximation, however, is known to be not even qualitatively correct. Summing the series for  $f$ , even with an approximate form for the potential, we can take account of all multiple scattering terms. This is automatically done by solving the Schrödinger equation exactly (say by a coupled channel procedure). Alternatively the approximate potential may be inserted into Glauber's multiple scattering expansion.

An alternative approach which has been extensively used for analysing high energy nucleon scattering and provides a direct link of the scattering amplitude  $f(\vec{k}, \vec{k}')$  to nuclear structure quantities e.g. to nucleonic distributions, is Glauber's multiple scattering approximation [Glau 59-69, Ba Wi 68, Au Lom 74, Lo Wi 75]. This model expresses  $f(\vec{k}, \vec{k}')$  in terms of the projectile - target nucleon (two-body) amplitude  $t$  by a multiple scattering series, in the case of elastic scattering averaged over the distribution of the nucleons.

In the impact parameter description the scattering amplitude takes the following form

$$f(q) = \frac{ik}{2\pi} \int e^{i\vec{q}\vec{b}} \Psi_f^*(\vec{r}_j) \Gamma(\vec{b}, \vec{S}_1 \dots \vec{S}_A) \Psi_i(\vec{r}_j) d^3 r_1 \dots d^3 r_A d^2 b \quad (1.6)$$

Here  $k$  is the incident momentum,  $d^2 b$  the element of area in the impact vector plane,  $\Psi_i$  and  $\Psi_f$  the initial and final nuclear states. The Glauber model is based on the dynamical approximation that the phase function  $\chi_A(\vec{b})$  defining the total profile function

$$\Gamma(\vec{b}) = 1 - e^{i \chi(\vec{b})} \quad (1.7a)$$

is the sum of the phases of the individual scatterers  $\chi_j(\vec{b}-\vec{S}_j)$  with  $\vec{S}_j$  representing the position of the  $j^{\text{th}}$  nucleon. Thus we have

$$\Gamma(\vec{b}, \vec{S}_1, \dots, \vec{S}_A) = \prod_j \Gamma_j(\vec{b}-\vec{S}_j) = \prod_{j < m} \Gamma_j(\vec{b}-\vec{S}_j) \cdot \Gamma_m(\vec{b}-\vec{S}_m) \dots \quad (1.7b)$$

Assuming the Fermi motion of the nucleus to be small with respect to the incident momentum the matrix element can be calculated from the particle-target nucleon amplitude  $t_j(q)$  (which provides  $\Gamma_j$  via a Fourier transformation (1.6)).

In the past decade the first order expression for the optical potential

$$U(\vec{r}_p) = \int v_{\text{eff}}(\vec{r}-\vec{r}_p) \rho_m(\vec{r}) d^3r \quad (1.8a)$$

with

$$\rho_m(\vec{r}) = \langle 0 | \sum_{i=1}^A \delta(\vec{r}-\vec{r}_i) | 0 \rangle \quad (1.8b)$$

has been extensively used. The procedure worked out by Greenlees et al. [Green 68] for medium energy nucleon scattering is designated as the *folding model* or *reformulated optical model* (ROM). The remarkable success of the Greenlees approach inspite of some obvious drawbacks due to the neglect of the higher order terms and of an explicit treatment of exchange in the early simplified form - has revived the interest in medium energy particle scattering and stimulated the application to the scattering of strongly observed complex projectiles, even to heavy ions [Var Do 73, Do Var 74]. The attractive feature of such an approach is that it seems to open a convenient door to the information of interest, once the effective interaction is determined. In its original form the scattering operator is nonlocal and energy dependent. It differs also from the free interaction. In view of these difficulties and following a standard procedure the projectile-bound nucleon amplitudes  $\{t_j\}$  are replaced by a local effective interaction. Usually some phenomenological adjustments are necessary in order to fit the experimental data as a quantitative microscopic theory, in particular of nucleus-nucleus interactions is somewhat beyond our reach at present. Hence folding models are a compromise which retains the more important physical features but have to be flexible enough to include implicitly what is only accessible in a phenomenological way.

We present here a sample of results based on such interaction models generating the optical potential by averaging an effective projectile-bound nucleon interaction over the nucleon density distribution, in some cases with some corrections of the primary simplifications of the models. We endeavour to outline the area of confidence and uncertainty in determining size and shapes of nuclei.

## 2. ELASTIC NUCLEON SCATTERING

In their analyses of elastic scattering of 14.5, 30.3 and 40 MeV protons by a range of nuclei and with the motivation of studying the density distributions of the target nucleons, Greenlees et al.

[Green 68-70] synthesized the real central part of the optical potentials by a Yukawa NN force with an appropriate exchange mixture and by a Fermi function parametrization of the matter distribution

$$\rho_m(r) = \rho_p + \rho_n = \rho_o \left[ 1 + \exp \left( -\frac{r-c_m}{a_m} \right) \right]^{-1} \quad (2.1)$$

The real central part

$$U_R(r_p) = \int \rho_m(r) V_d(\vec{r}-\vec{r}_p) d^3r + \int [\rho_n(r) - \rho_p(r)] V_\tau(\vec{r}-\vec{r}_p) d^3r \quad (2.2)$$

has a volume term which follows the nuclear density but is smeared by  $V_d$ , and an isospin potential which depends on the difference  $\rho_n - \rho_p$  and the isospin dependent part  $V_\tau$  of the NN interaction.

As variable parameters the half-way radius  $c_m$  and the diffuseness  $a_m$  of the matter distribution together with the central and spin-orbit formfactor strengths, respectively, and the parameters associated with the phenomenological absorption term are taken. The fits to the data in energy range considered were strikingly good and have been improved by relaxing the assumption  $\rho_p = \rho_n$  and allowing the protons and neutrons to have different distributions ( $\rho_p$  fixed by electromagnetic results). The most important observation was that, although the individual geometrical parameters could take a wide range of values, the rms radius of the real central potential was well defined. For a given range of the two-body force, nuclear rms radii ( $\langle r^2 \rangle_U = \langle r^2 \rangle_m + \langle r^2 \rangle_{V_{eff}}$ ) were obtained the values of which proved to be considerably larger than corresponding rms radii derived from electron scattering or muonic X ray experiments, thus implying large neutron-proton rms radii differences. Obviously such conclusions depend on the range of the assumed

effective interaction. Unfortunately the experimental cross sections are rather insensitive to the range parameter of the NN force and even to the type of interaction. In the case of  $^{208}\text{Pb}$ , e.g. the resulting neutron-proton rms radii differences vary from 0.46 fm for a Yukawa force with  $\langle r^2 \rangle_{V_{\text{eff}}}^{1/2} = 1.5$  to 0.13 fm for a Gaussian force with  $\langle r^2 \rangle_{V_{\text{eff}}}^{1/2} = 2.07$  fm. Subsequent work [Green 70ab] using a more detailed and improved approach (with explicit isospin term and folded spin-orbit term) prefers a Gaussian interaction ( $\langle r^2 \rangle_{V_{\text{eff}}}^{1/2} = 2.07$  fm) deduced by an analysis of low energy np and pp data. The revised values of the neutron skin thickness  $\langle r^2 \rangle_n^{1/2} - \langle r^2 \rangle_p^{1/2}$  are about zero for Ni and Fe nuclei and increasing to ca. 0.15 fm for  $^{120}\text{Sn}$  and  $^{208}\text{Pb}$ .

Here we realize the general uncertainty we are worrying about in deriving information about the nuclear matter distribution unless we have complete confidence in the effective interaction used and are satisfied that the corrections are negligible. Following the initiating work the Greenlees approach has been discussed and refined in several theoretical studies [Sl Mc 68, Fri 69, Ki Ro 70, Th Sin 71, Th 73] in order to reduce uncertainties and to obtain a clearer understanding of the necessary corrections and the significance of the results. The main effects considered are the following

- a) Exchange effects arising from antisymmetrisation between projectile and target nucleons and represented by a (nonlocal) exchange potential which contributes significantly to the 30 MeV proton optical potential [Ow Sa 70] and changes the potential rms radius.
- b) Off-shell effects [Le Ri 72].
- c) Dependence on various types of interactions: realistic and density dependent forces [Sl Mc 68, Th 73].
- d) Effects due to the particular treatment of the absorptive part, second order effects and contributions from inelastic [Mac 71] and reaction (pick-up) channels [Ma Ko 76].

The various aspects have been recently reviewed and summarized by Sinha [Sin 75] by refining the approach in some details and emphasizing the importance of using an effective interaction with correct saturation properties ("bound state" interaction rather than the free interaction) We may conclude that the essential idea behind the folding procedure for medium energy nucleon scattering can be regarded to be justified

though there are many delicate sensitivities and dangers in attempting to derive nuclear density information. Indeed with view to the complications affecting the interpretation of medium energy nucleon scattering in terms of the nuclear matter distributions, the Greenlees approach has lost much of its original appealing simplicity. This may be one reason that after the first impact nucleon scattering below 100 MeV is not often applied as tool for a serious empirical investigation of nuclear matter distributions apart from studies of the reaction model itself.

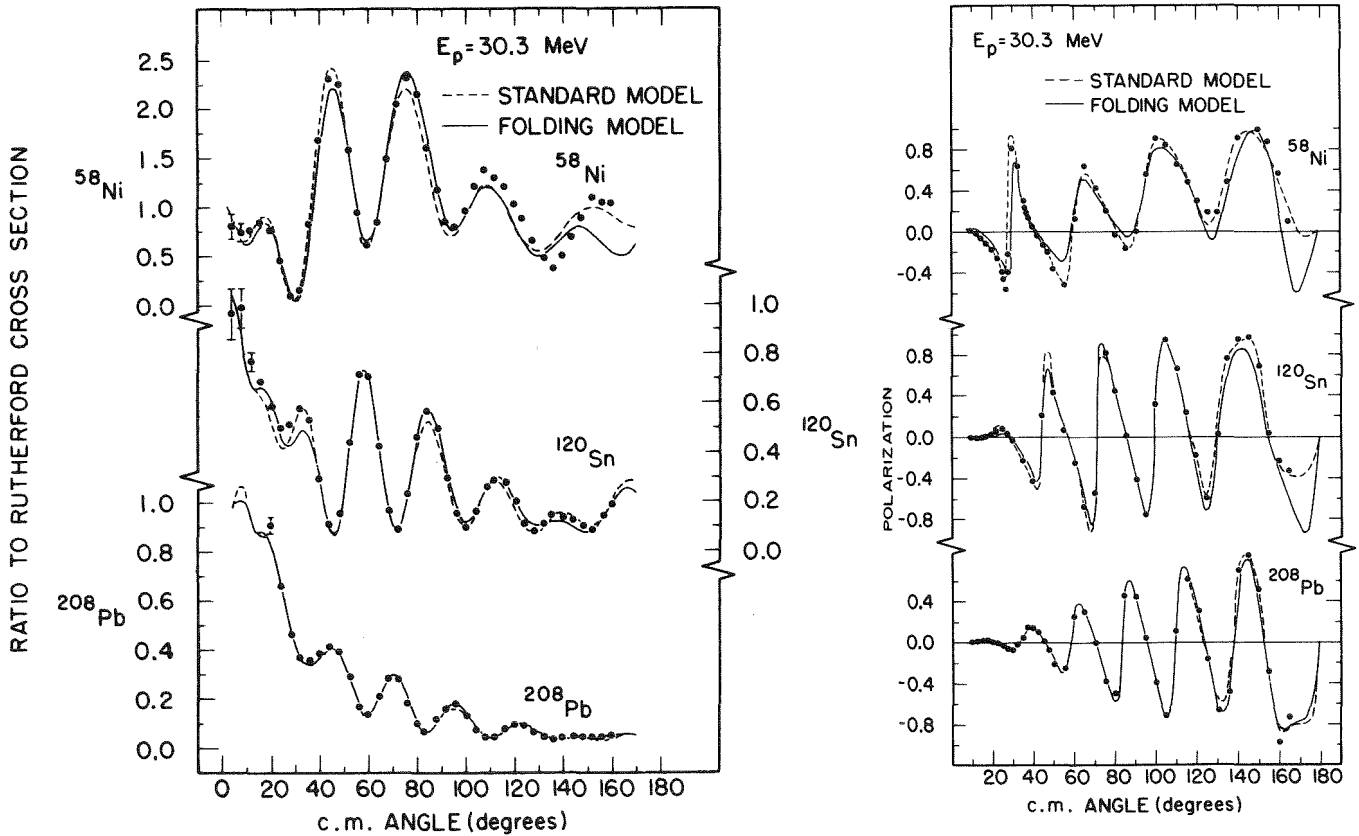


Fig. 1: Angular distribution and polarization of elastic scattering of 30 MeV protons [Green 70]. The calculations on the basis of the phenomenological standard model and the folding model describe the experimental data equally well.

An early analysis of the elastic scattering of neutrons by a range of nuclei resulted in neutron-proton rms radius differences of ca. 0.5 fm [Ho Wi 68]. Some uncertainties are ruled out by considering merely isotopic differences as done for the Sn and Ca isotopes [Boy 71, Boy Gr 68, Lomb 72]. The procedures analyze adequately constructed isotopic difference functions of the experimental data in order to increase the sensitivity to matter radius variations.

Will higher energies of the incident nucleons help to disentangle the interaction of the probe and the structure of the probed nucleus? High energy reactions have often been claimed to be a convenient way of measuring the nucleon distributions in nuclei. The general arguments are based on some expected simplifications of the scattering process. A low energy proton introduced into a nucleus participates in the many body dynamics, and there is little to distinguish it from one of the target nucleons. On the other hand a high energy particle passing through the nucleus is on the average hardly deflected. Its momentum is much greater than the typical Fermi momenta in the nucleus, and it will have left the nucleus before the induced nuclear rearrangement can take place. In the main the target nucleons are just spectators, and in a first approximation the scattering problem is a sequence of two-body interactions. In other words the impulse approximation which has been used for many years to construct an optical potential for nucleon-scattering at intermediate energies provides a reasonable procedure if applied with some corrections due to double scattering and including a realistic description of two-nucleon correlations. At even higher energies the use of the free two-body interaction  $f_{NN}(q)$  is suggested so that the first order optical potential becomes

$$U(r) = \int e^{i\vec{q}\cdot\vec{r}} F_m(q) f_{NN}(q) d^3q \quad (2.3)$$

We realize that in some certain aspects high energy proton scattering takes many features which are fortunately found when probing the nucleus by electron scattering. Of course, we must not forget that the basic force is in many of its details largely unknown. The force is strong and its strength is such that the probing proton will interact with several nucleons on its traverse of the nucleons and it will be influenced by any correlations among the target nucleons. These cause virtual excitations of the nucleus (dispersion effects) which should be of some importance. The framework of the theoretical analysis follows either the approach of Kerman, McManus & Thaler (KMT) or the

Glauber approximation. Until recently, however there have been only few attempts to determine the nucleonic distributions directly from experiments. Together with inaccuracies related to the description of the scattering processes the minor quality of the experimental data prevented clear information. Now, recent experiments done at Gatchina [Alk 72] and at Saclay [Berti 73] continuing the pioneering work of many groups (see the recent review of Saudinos and Wilkin [Sa Wi 74]) provide an excellent experimental basis. Elastic and inelastic scattering of 1 GeV protons has been studied with spectrometers of improved resolution, sometimes as good as 100 keV (Saclay). The theoretical analyses are characterized by a more detailed and quantitative aspect as previous work. Both the Glauber approach and the Kerman-McManus-Thaler one (also including Feshbach second order term) necessitate some knowledge of the nucleon-nucleon scattering amplitude which is presently very scarce (spin part of the NN amplitude). Usually the (scalar) nucleon-nucleon amplitude is parametrized by

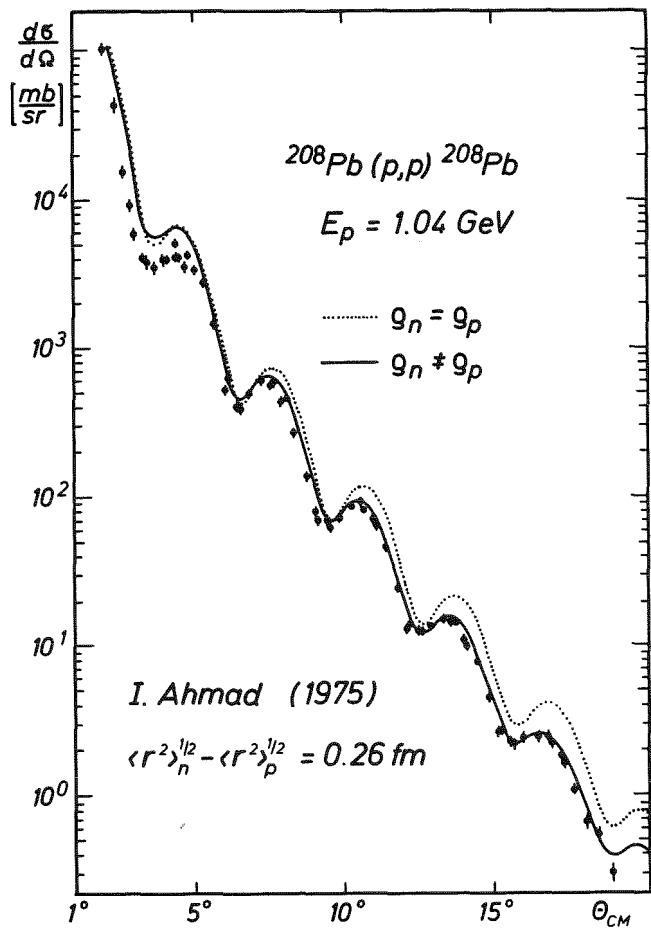


Fig. 2: Elastic proton scattering by  $^{208}\text{Pb}$  at 1.04 GeV. The theoretical curves are results of an analysis based on the Glauber theory [Ahm 75]

$$f_{NN}(q) = \frac{i + \alpha}{4\pi} k \cdot \sigma_T \exp(-\beta^2 q^2/2) \quad (2.4)$$

where  $\sigma_T$  is the total nucleon-nucleon cross section,  $\alpha$  the ratio of real to imaginary part of  $f_{NN}(q)$  and  $\beta^2$  the slope of the NN differential cross section.

The experimental cross sections for 1 GeV proton scattering show distinct diffraction pattern (fig. 2) and resemble to complex particle scattering with strong absorption at the nuclear surface. The analyses, in particular of the  $^{208}\text{Pb}$  and  $^{48}\text{Ca}$  data (measured by the Saclay and Leningrad group, respectively) involve differences between neutron and proton density distributions. Auger and Lombard [Au Lom 74] obtain good results with Hartree Fock densities. Recently the detailed studies of Ahmad [Ahm 75] yield a neutron-proton rms radii difference of 0.26 fm for  $^{208}\text{Pb}$  which is consistent with results of various other methods (see sect. 3). The larger mean radius of the neutron distribution is ascribed to a larger value of the surface diffuseness (see Gla Ma 70). The effect is demonstrated in fig. 2. But it is not clear yet if a change of the diffuseness is the only possibility to adjust the general slope of the differential cross sections. In  $^{48}\text{Ca}$  the surface envelope of the neutron distribution is found to be the same as for the proton distribution but is placed at a larger radius.

Very accurate high energy data are also available for the total cross sections of neutron nucleus scattering (see Fran 72 and references there). The data for incident momenta of 1.5-30 GeV/c have been studied by Franco [Fran 72] concluding that the region around  $c_m$ - $a_m$  contributes mainly to  $\sigma_{\text{Tot}}$ .

Although there are some limitations which we hope to be removed by further theoretical advances intermediate energy proton-nucleus scattering experiments provide rich information on matter ground state as well as on transition densities (and correlations in light nuclei). Looking with eyes charmed with the uniqueness of electromagnetic information we are careful in making too precise statements until all the details of the scattering process have been taken into account. Nevertheless using empirically-determined NN amplitudes to interpret p-nucleus elastic scattering we may rather confidently relate the surface structure of the nuclear matter distribution to the scattering cross sections.

### 3. ELASTIC SCATTERING OF STRONGLY ABSORBED PARTICLES

#### 3.1 Folding model approach

The folding model approach has been applied successfully to the scattering of complex projectiles, in particular to the scattering of  $\alpha$ -projectiles <sup>\*)</sup>. In many aspects  $\alpha$ -scattering seems to be considerably more reliable than medium energy nucleon scattering. Since the interaction is isoscalar the range of the phenomenological two-body interaction may be determined in light nuclei where proton and neutron densities are almost identical [Bern 71, Lern 72], and then used with confidence. Due to the strong absorption in the nuclear surface the elastic channels probe only the nuclear surface in a low density region where the multiple scattering expansion is expected to converge, and it is plausible that the relation between density and optical potential at the nuclear surface is rather independent of the specific nucleus. That implies that the effective  $\alpha$ -nucleon interaction is expected to be not very different from the free interaction and that effects due to exchange and antisymmetrization are of minor importance and may be taken into account by simple approximations. Exploiting these obvious advantages various procedures have been worked out differing in the types of effective interactions used: phenomenological  $\alpha$ -nucleon potentials [Mail 72, Mail 74, Si 75] or in a more symmetric (finally a double folding) approach an effective interaction generated from the long range part of the nucleon-nucleon interaction [Ja Ke 69, Bern 69b, Bud 70, Bat 71]. According to Batty et al. [Bat 71] the best choice for a local effective interaction is of the most convenient Gaussian form

$$V_{\text{eff}}(\vec{r}, \vec{r}_\alpha) = \lambda_R(E) \cdot V_0 \exp \left[ -|\vec{r} - \vec{r}_\alpha|^2 / \mu_0^2 \right] \quad (3.11)$$

The strength  $V_0$  and the range  $\mu_0$  are derived by averaging the nucleon-nucleon interaction over the internal motion of the  $\alpha$ -particle. The energy-dependent factor  $\lambda_R(E)$  allows some phenomenological adjustment of the free  $\alpha$ -nucleon interaction due to the influence of the bound nucleons. As proposed by Bernstein [Bern 71] the quantity  $\lambda_R$  can be

<sup>\*)</sup> A comprehensive review of the scope of various efforts and procedure is given in [Re 74c].

determined by calibrating the effective interaction by  $\alpha$ -particle scattering from light nuclei, in particular from  $^{40}\text{Ca}$ . As suggested by Schaefer exchange effects can be represented by the addition of a shorter range pseudo potential [Schae 70]. The case of 104 MeV  $\alpha$ -particle scattering has been investigated in detail [Gi Re 75a] considering various sensitivities and including empirical studies of exchange effects on the basis of Schaefer's approximation. It has been pointed out that for 100 MeV  $\alpha$ -particle scattering in the diffraction region the exchange effects are absorbed by the phenomenological factor  $\lambda_R$ . As shown by Batty et al. there is a parameter ambiguity of the Gaussian interaction obeying the relation:  $\lambda_R \cdot V_O \cdot \mu_O^6 = \text{const}$ . Most of the following  $\alpha$ -particle scattering examples use a set of parameter values:  $\mu_O = 1.95 \text{ fm}$  and  $\lambda_R \cdot V_O = 40 \text{ MeV}$ .

For the imaginary part  $U_I(\vec{r}_\alpha)$  of the optical potential the usual macroscopic Saxon-Woods representation has been used with parameters adjusted in fitting the cross sections. Alternatively a procedure taking  $U_I \propto U_R$  or a derivative of the real part has been used [see Ber Pa 76].

### 3.2 Nuclear size information from elastic $\alpha$ -particle scattering in the 100 MeV region

As an example we discuss briefly a recent investigation of elastic  $\alpha$ -particle scattering from  $^{204,206,208}\text{Pb}$  at  $E_\alpha = 104 \text{ MeV}$  [Gi Re 76]. The neutron distributions and isotopic differences of the rms radii have been investigated by adopting proton distributions from precise electron scattering experiments\* [Eu 76] with momentum transfers  $q < 2.5 \text{ fm}^{-1}$  and fitting the neutron distribution to  $\alpha$ -particle scattering cross sections (fig. 3). The analyses result in substantial neutron-proton rms radii differences

$$\begin{array}{rcl} \langle r_n^2 \rangle^{1/2} - \langle r_p^2 \rangle^{1/2} & = & \begin{array}{l} 0.30^{+0.07} \text{ fm} \quad ({}^{208}\text{Pb}) \\ 0.19^{+0.09} \text{ fm} \quad ({}^{206}\text{Pb}) \\ 0.22^{+0.09} \text{ fm} \quad ({}^{204}\text{Pb}) \end{array} \end{array}$$

\*) Possible effects of the neutron charge distribution have been assumed to be negligible and are expected to be less important at  $q < 3.0 \text{ fm}^{-1}$  [Bert 72]

Some details of these studies are of particular interest:

- a) As suggested by the electron scattering results the neutron distributions are parametrized by a modified Gaussian form

$$\rho_n = (1+w_n \frac{r^2}{c_n^2}) \left[ 1 + \exp((r^2-c_n^2)/a_n^2) \right]^{-1} \quad (3.21)$$

rather than by a Fermi form. There are indications that the description of the  $^{208}\text{Pb}(\alpha,\alpha)$  cross sections is improved by use of such a parametrization.

- b) As shown by the  $\chi^2$ -contour plots in the inset of fig. 3 various correlations between the phenomenological parameters  $c_n$ ,  $a_n$  and  $w_n$  have been studied.

The curves represent sections through the  $\chi^2$  minimum point enveloped by the hypersurface  $\chi^2 = 1.5 \chi^2_{\text{min}}$ . Obviously there is a correlation between  $c_n$  and  $w_n$  allowing both parameters to vary over a wide range provided that the combination of  $c_n$  and  $w_n$  reproduces a stable value of the rms radius. The parameter  $a_n$  in this case does not essentially influence the resulting rms radius.

- c) By careful studies of the surface localization of  $\alpha$ -particle scattering the part of the density distribution which is sensitive to the cross sections is determined. All possible parameter correlations require nearly identical slopes of  $\rho_n$  at the surface  $r > 6.5$  fm (see fig. 4).
- d) In the case of  $^{208}\text{Pb}$  there seems to be a strong tendency of preferring a neutron density distribution with a slope steeper (diffuseness smaller) than that of the proton distribution or as compared to the  $^{204,206}\text{Pb}$  cases. This does not agree with the conclusions from 1.04 GeV proton scattering [Ahm 75] analysed in terms of a Fermi distribution with a larger neutron density diffuseness  $a_n$  and the halfway radii  $c_n = c_p$ . Experiences with parametrized phase shift analyses, however, indicate that the observed differences between the theoretical  $(\alpha,\alpha)$  cross section calculated with  $\rho_n = \rho_p$  (see fig. 6) and the measured cross section are characteristic for larger  $c_n$  and smaller  $a_n$  values. Similarly one may argue that a comparison of the heights of corresponding diffraction maxima of different Pb isotopes suggests that  $^{208}\text{Pb}$  has a smaller diffuseness than the two other Pb isotopes.

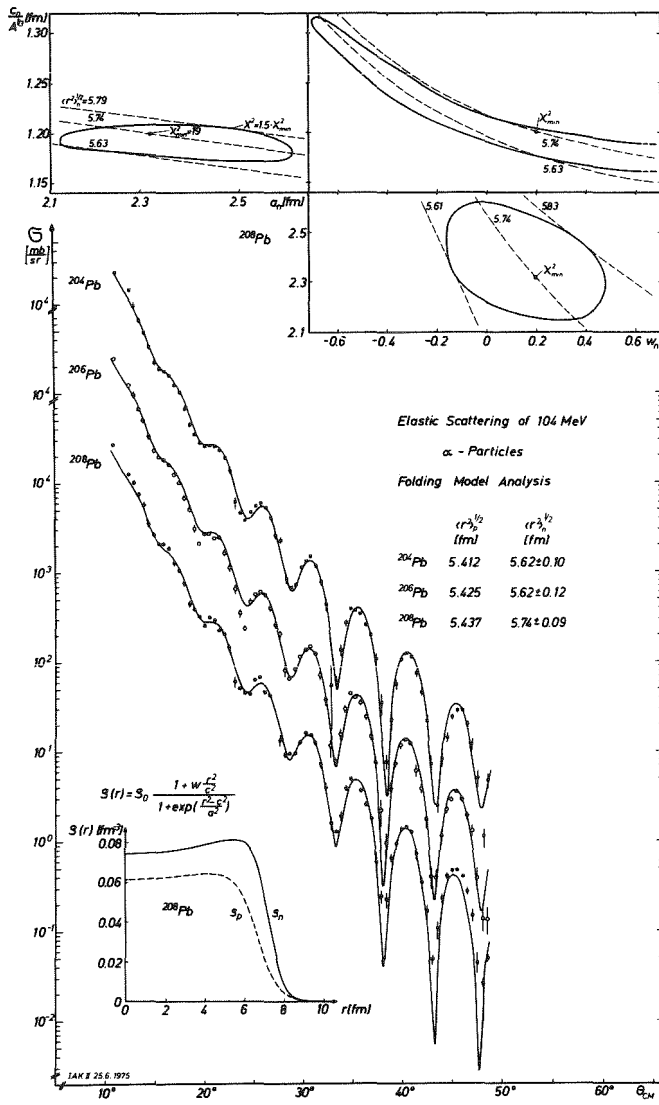


Fig. 3: Folding model analyses of  $^{204}, ^{206}, ^{208}\text{Pb}(\alpha, \alpha)$  cross sections at  $E_\alpha = 104$  MeV using different distributions for protons and neutrons. The upper inset displays  $\chi^2$ -contour plots in various planes of the parameters of  $\rho_n$ .

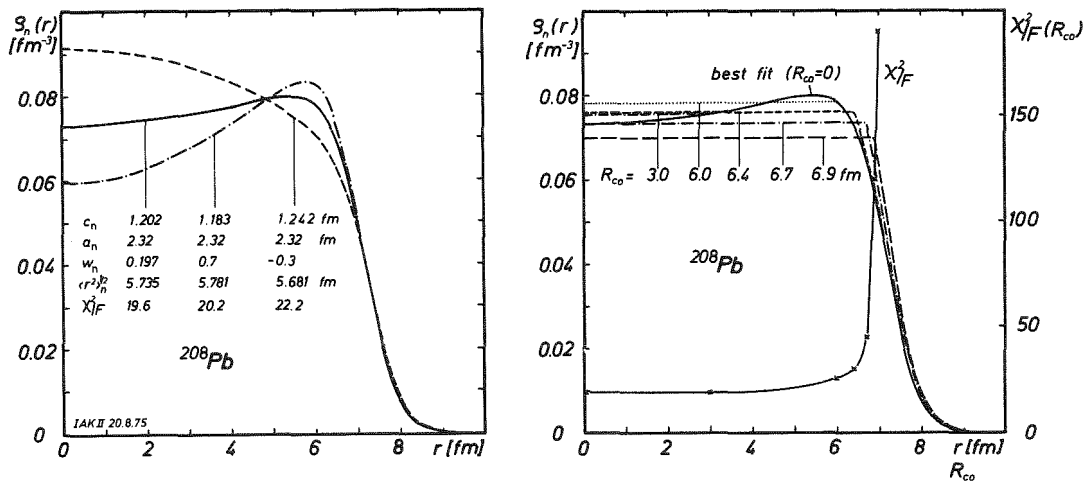


Fig. 4: Neutron distributions of  $^{208}\text{Pb}$  obtained with constraints to the parametrization. (a) Parameters  $a_n$  and  $w_n$  fixed,  $c_n$  adjusted. (b)  $\rho(r) = \text{const.}$  for  $r < R_{co}$ ,  $\rho(r) = \rho(c_n, a_n, w_n, r)$  for  $r > R_{co}$ ;  $c_n, a_n, w_n$ : best fit parameters. The curve showing the dependence of the  $\chi^2$  values from  $R_{co}$  is scaled on the right/hand ordinate.

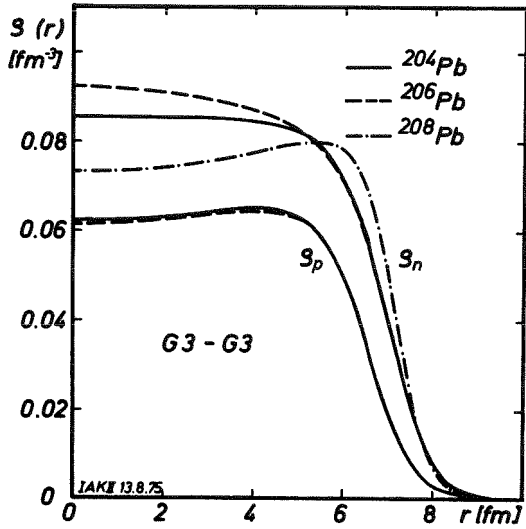


Fig. 5: Proton and neutron distributions of  $^{204}, ^{206}, ^{208}\text{Pb}$ . The distributions are parametrized by a modified Gaussian form (G3).

A	$\langle r_{ch}^2 \rangle^{1/2}$ [fm]	$\langle r_p^2 \rangle^{1/2}$ [fm]	$\langle r_n^2 \rangle^{1/2}$ [fm]	$\langle r_p^2 \rangle^{1/2} \langle r_n^2 \rangle^{1/2}$ [fm]
204	5.4722	5.4120	5.62(10)	0.21(10)
206	5.4845	5.4245	5.62(12)	0.20(12)
208	5.4967	5.4368	5.735(85)	0.298(85)

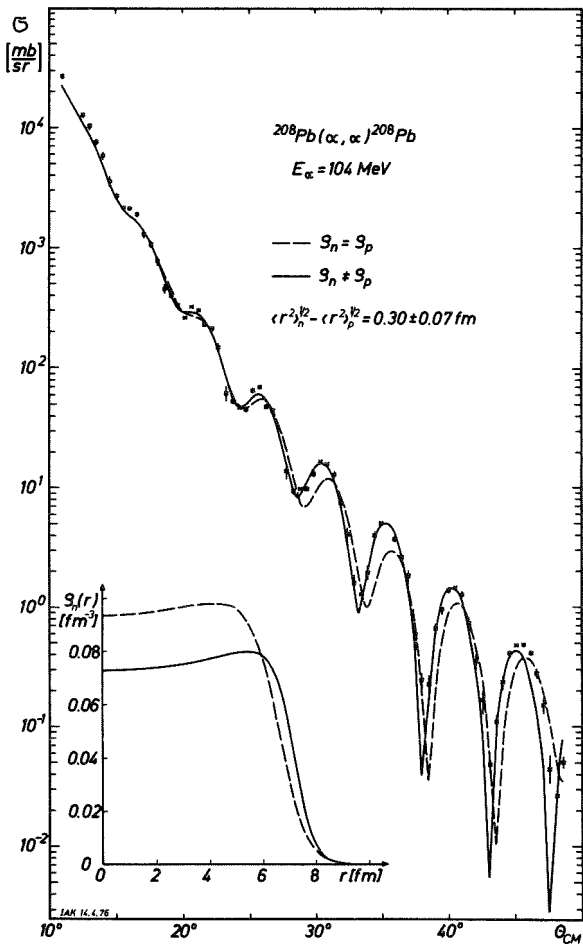


Fig. 6: Elastic differential cross sections of 104 MeV  $\alpha$ -particle scattering from  $^{208}\text{Pb}$ :  
 -----  $\rho_n = \rho_p$   
 \_\_\_\_\_  $\rho_n \neq \rho_p$

Recent theoretical studies [Yar 76] considering the single particle spectra of  $^{208}\text{Pb}$  conclude for the single particle potentials  $a_p > a_n$ . Tab. 2 presents a survey of the results obtained for  $^{208}\text{Pb}$  in various analyses and by different approaches. We may consider with greatest confidence those methods which are most extensively established by the improving process of frequent applications. Such arguments clearly favour medium energy nucleon and  $\alpha$  particle scattering, matured and refined by many systematic studies covering light and heavy nuclei (see for example fig. 7). It is encouraging that there seems to be an increasing consensus that the nuclear matter distribution of  $^{208}\text{Pb}$  distinctly exceeds the proton distribution at the surface. But there are also indications -  $\pi^\pm$ -reaction cross sections and high energy photo pion production - which seem to conflict with the results of the other methods. It is fair to say that for these methods though offering a tremendous potential for a systematic study of the neutron distributions, the empirical applicability is not sufficiently well established, presently.

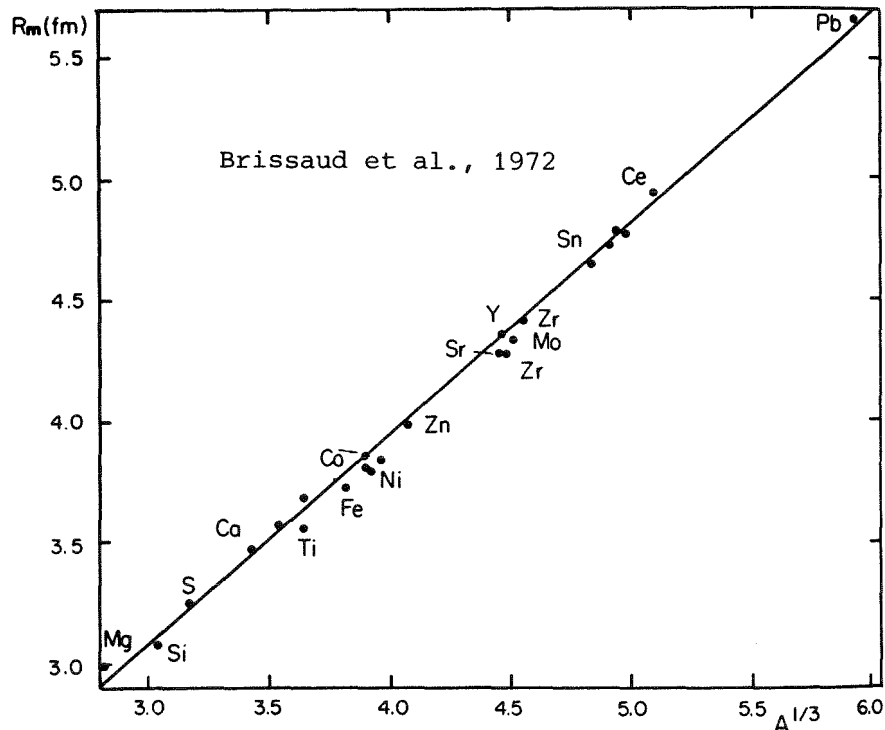


Fig. 7: Nuclear matter rms radii varying with  $A^{1/3}$  as found by a systematic investigation of elastic  $\alpha$ -particle scattering at  $E_\alpha = 166 \text{ MeV}$  [Bri 72]

Method	$\langle r^2 \rangle_m^{1/2}$ [fm]	$\Delta r$ [fm]	Reference
$\alpha$ -scattering 79 MeV	$5.53 \pm 0.10$		Ru Hi 76
104 MeV	$5.59 \pm 0.06$	$0.26 \pm 0.13$	Bern 72
104 MeV	$5.63 \pm 0.05$	$0.30 \pm 0.07$	Gi Re 76
140 MeV	$5.69 \pm 0.10$	$0.42 \pm 0.20$	Bern 72
166 MeV	$5.65 \pm 0.10$	$0.25 \pm 0.09$	Tat 72
$p$ -scattering 30 MeV	$5.66 \pm 0.20$	$0.36 \pm 0.20$	Green 70b
1.04 GeV		$0.26 \pm 0.10$	Thir 74 -Ahm75
19.3 GeV/c	5.49		Gla Ma 70
Coherent ( $\gamma, \pi^0$ )	$5.78 \pm 0.30$		Schra 62
Coherent ( $\gamma, g^0$ )	$5.66 \pm 0.15$	$0.31 \pm 0.15$	Alv 70
$\zeta(\pi^+)/\zeta(\pi^-)$ 800 MeV		$-0.11 \pm 0.11$	Au 68
0.7-2.0 GeV/c		$0.0 \pm 0.1$	Alla 73
$(\gamma\pi^-)/(\gamma\pi^+)$ 8/16 GeV		$-0.7 \pm 0.4$ (halfway rad.)	Boj 69
Coulomb displacement energy		0.115	No Sch 69
Subcoulomb n-pickup		0.1-0.2	Kö Sch 71
Strong absorption radius interpretation (42 MeV $\alpha$ -scat)	5.55		Sum 74
Rutherford radius interpretation ( $\alpha$ -scattering n.Coul. b.)	5.48	0.-0.12 <0.1	Ba Li 74 Bat Fri 71
$K^-$ absorption		$0.44 \pm 0.16$	LeSe 74
$\bar{p}$ -absorption		0.1 to 0.7	Bug 73
HF prediction	5.51	0.23	Neg70
Electron scattering	$\langle r^2 \rangle_p^{1/2} = 5.43 \pm 0.03$		Eu 76

Tab. 2:  $^{208}\text{Pb}$  rms radii and neutron-proton differences  $\Delta r$

It should be noted that most of the methods are probing only a restricted part of the density distribution, e.g. referring primarily to the outer tails of  $\rho_m(r)$  and the relying massively on an anticipated phenomenological form to relate those tails to the rms radii. This may imply additional uncertainty and discrepancies when comparing with results referring more directly to the main body of the matter distribution.

As demonstrated e.g. by Bernstein and Seidler [Bern 72] for the case of 104 MeV elastic  $\alpha$ -particle scattering from  $^{90}\text{Zr}$  the analyses using phenomenological parametrizations (Fermi shapes) of  $\rho_m$  determine the rms radius much better than the parameters of the adopted functional form. The relatively large range of possible values of the parameter combinations effects the well marked uncertainty of the value of the central density  $\rho_0$ . Physically, this is the consequence of the strong absorption. It has been proposed [Mac 76] to eliminate parameter sets apparently unphysical in the nuclear interior by introducing suitable constraints e.g. for  $\rho_0$ . Obviously the surface region is rather well determined (fig. 8). These features remind of a somewhat similar behavior of the tails of the optical potentials. The observation that a region around a certain prominent value of  $r$  is rather insensitive to the parameter uncertainties may be induced by the lack of flexibility of the particular form.

In order to overcome the drawbacks of phenomenological parametrizations of  $\rho_m(r)$  some recent analyses [Bri Br 76, Lo Wi 76] apply "model independent" techniques originally worked out for electron scattering analyses [Sic 73]. In the framework of the assumed reaction model they

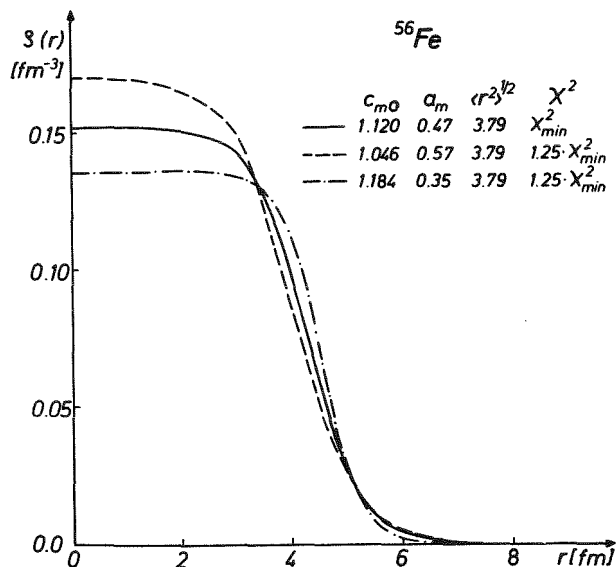


Fig. 8: Radial Fermi shapes calculated from different sets of  $c_m$  and  $a_m$  extracted from 104 MeV  $\alpha$ -particle scattering by  $^{56}\text{Fe}$  [Gi Re 75b]

reveal the uncertainties of each point and of the radial moments  $R_K = \left\{ \frac{1}{A} \int \rho_m(r) r^{K+2} \right\}^{1/K}$  of the nuclear matter distribution  $\rho_m(r)$ . It is interesting to note that proton scattering at 1 GeV and  $\alpha$ -scattering at about 100 MeV appear to have similar information content. These studies confirm the previous statements [Bern 72, Gi 74, Gi 75] that the moments like the rms radius ( $K=2$ ) are very well determined (with uncertainties comparable to those obtained in model dependent analyses of electron scattering) despite of the considerable uncertainties of  $\rho_m(r)$  at small radii.

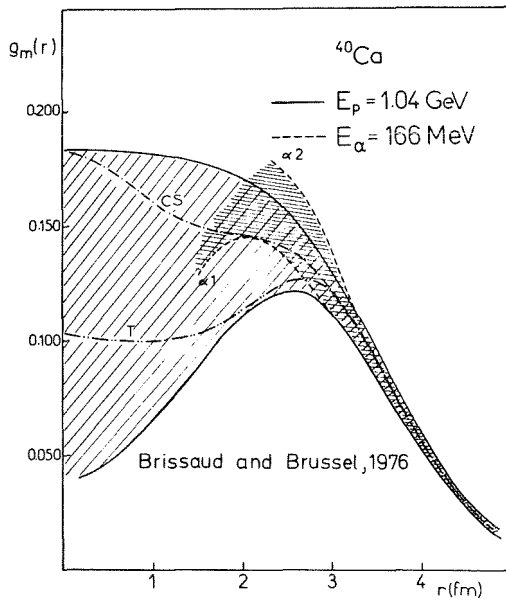


Fig. 9: Envelopes of trial densities resulting from "model independent" analyses of  $\alpha$ -particle ( $\alpha_1$ - $\alpha_2$ ) and proton scattering [Bri Br 76].  
 T : typical density  
 CS: theoretical density [Ca Sp 72]

### 3.3 Information from strong absorption radii and from elastic scattering at energies near the Coulomb barrier

Because of the ambiguities possible for strongly absorbed projectiles, the half-way radius and the equivalent-radius of the optical potential extracted by the usual phenomenological procedures cannot be regarded as significant size parameters. The *strong absorption radius*  $R_{FC}$  and the real potential  $U_R$  at that radius, however, appear to be very well determined quantities [Ja Mo 68, Fern 70] and are accessible to a microscopic interpretation in terms of the nuclear matter distribution. The strong absorption radius  $R_{FC}$  is defined as

$$kR_{FC} = \eta + (\eta^2 + L_c(L_c + 1))^{1/2} \quad (3.31)$$

where  $\eta$  is the Coulomb parameter and  $L_C$  the critical angular momentum:  $\text{Re}(S_L) = 1/2$  with  $S_L$  being the reflection coefficients determined by a direct parametrization of the phase shifts or alternatively, generated by the optical potential.

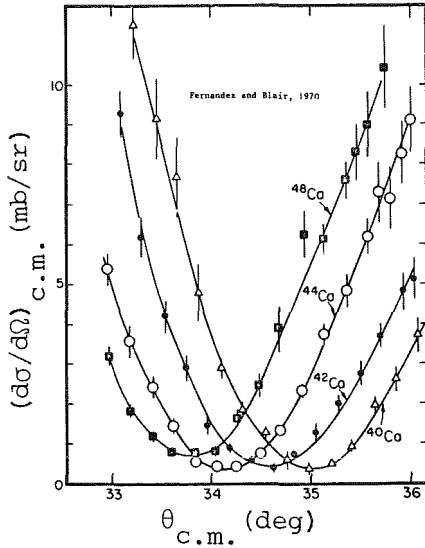


Fig. 10: Angular distributions for elastic scattering of 42 MeV  $\alpha$ -particles by the Ca isotopes in the region of the minimum at  $35^\circ$  |Fern 70|

This type of *interaction radii* is mainly determined by the first oscillations in the angular distributions of elastic  $\alpha$  particle scattering. There have been considerable efforts in determining such radii empirically with high accuracy, especially regarding the variations of the diffraction radii of neighboring isotopes |Fern 70|.

Isotope	$E_{\text{Lab}}$ [MeV]	$R_{\text{FC}}$ [fm]	$R(U_R = - 2.4 \text{ MeV})$ [fm]
$^{40}\text{Ca}$	42.10	$7.415 \pm 0.02$	7.415
$^{48}\text{Ca}$	42.10	7.58	7.58
$^{204}\text{Pb}$	41.99	10.34	10.38
$^{206}\text{Pb}$	42.27	10.42	10.43
$^{208}\text{Pb}$	42.25	10.52	10.53

Tab. 3: Strong absorption radii for 42 MeV  $\alpha$ -particle scattering |Sum 74|

As verified by Goldring et al. |Gol 70| there are "invariant" quantities similar to  $R_{\text{FC}}$  and  $U_R(r = R_{\text{FC}})$  also in cases where a diffraction radius does not exist. It has been pointed out that a detailed investigation of the elastic scattering of charged particles at incident energies near the Coulomb barrier can provide rather accurate information on relative sizes of isotopic nuclei. The method is essentially a refinement of the original Rutherford experiments in which the break

point from Rutherford scattering and the corresponding distance of closest approach were used as a measure of the size of the scattering nucleus. It has been shown that optical model analyses (or "incoming-wave boundary condition" analyses [Eis 72]) result in rather unambiguous values of two quantities: the maximum value of the total potential (barrier height  $V_B$ ) and the distance from the origin to the maximum potential (Rutherford radius  $r_R$ ). These quantities are primarily attributes of the nuclear potential.

For the analysis of the measured data the Coulomb potential is parametrized by the form of a homogeneous charged sphere and a Saxon-Woods form of the nuclear potential is assumed. Approximately we have

$$V_B \approx \frac{Z_1 Z_2 e^2}{r_R} \left(1 - \frac{a}{r_R}\right)$$

The values of  $V_B$  and  $r_R$  determined by elastic  $\alpha$ -particle scattering from  $^{204}\text{Pb}$ ,  $^{206}\text{Pb}$ ,  $^{208}\text{Pb}$  and  $^{209}\text{Bi}$  over the energy range 14 to 23 MeV [Gol 70] are given in tab. 4.

Barnett and Lilley [Ba 74] have measured  $(\alpha, n)$  cross section on  $^{208}\text{Pb}$  and  $^{209}\text{Bi}$  between 16 and 24 MeV and determined magnitude and shape of the real nuclear potential at a radial distance of about 11 fm by a detailed optical model analysis of the reaction data.

Target	$r_R$ [fm]	$V_B$ [MeV]	$R_{O2}$ [fm]	Ref.
$^{204}\text{Pb}$	10.88	20.54	11.91	[Gol 70]
	10.90	20.52	11.92	[Bad 74]
$^{206}\text{Pb}$	10.89	20.52	11.91	[Gol 70]
	10.89	20.54	11.91	[Bad 74]
$^{208}\text{Pb}$	10.94	20.42	11.96	[Gol 70]
	10.96	20.42	11.97	[Bad 74]
	10.9	20.49		[Ba Li 74]
$^{209}\text{Bi}$	$10.93 \pm 0.04$	$20.68 \pm 0.04$		[Gol 70]
	$11.01 \pm 0.08$	$20.63 \pm 0.08$		[Ba Li 74]

Tab. 4: Rutherford radii  $r_R$ , barrier heights and  $R_{O2}$  ( $V = -0.2$  MeV) values from  $\alpha$ -particle scattering

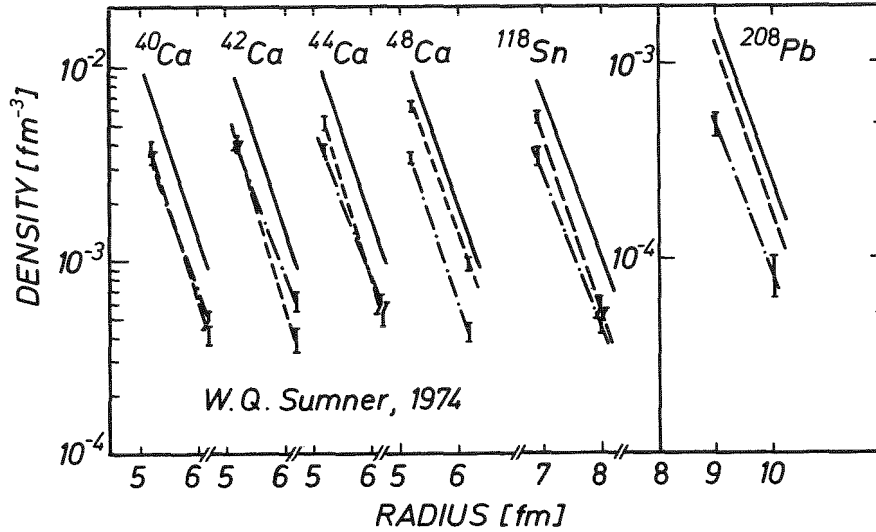


Fig. 11: Proton (---), neutron (----) and matter densities (—) derived by an unfolding procedure of the real interaction potential in the vicinity of the strong absorption radii for 42 MeV  $\alpha$ -particle scattering [Sum 74]. The proton densities are based on experimental charge distributions [Fro 68, Khv 70, Heis 69]

More recently Badaway et al. [Bad 74] have studied the  $\alpha$ -particle scattering by 23 isotopes of Cd, Sn, Re, Sm and Pb at energies near the Coulomb barrier. In an extensive analysis various sensitivities and the influence of the optical potential parameters, in particular, of the diffuseness  $a$  have been investigated. It turns out that the radius  $R_{02}$  where the nuclear potential has the value of  $-0.2$  MeV is better defined than the Rutherford radius  $r_B$ .

By use of elastic  $^{16}\text{O}$  scattering from  $^{40,44,48}\text{Ca}$  ( $E_{\text{Lab}} = 20-40$  MeV) the relative sizes of the Ca isotopes have been studied [Ber 71]. The resulting values of  $r_B$  vary approximately as  $A^{1/3}$  ( $r_B = 1.563 (16^{1/3} + A_T^{1/3})$  fm), in marked contrast to the observations of the charge radius [Bert 72]. This behaviour previously indicated by the diffraction radii deduced from 42 MeV  $\alpha$ -particle scattering [Bern 69a, Fern 70] (see fig. 10) has been confirmed by the  $^{16}\text{O}$  scattering experiments of Eisen et al. [Eis 72] while with  $^{18}\text{O}$  projectiles the situation is much less clear.

Recently isotopic differences of the even tin and neodymium isotopes [Tab 75, Tab 76] have been studied in detail by  $\alpha$  particle and  $^{16}\text{O}$  scattering. The region of the nuclear surface ( $R_{cf}$ ) where the (absolute) value of the nuclear potential is only 2 percent of the Coulomb potential is probed with maximal sensitivity. The size changes measured by  $\alpha$ -particle and by  $^{16}\text{O}$  scattering agree fairly well, but the increase of the radius  $R_{cf}$  (reflecting a corresponding increase of the matter size) is 2 to 3 times more rapid with neutron number than for the charge distribution sizes of the Sn isotopes [Barr 67, Ehr 68] (see fig. 12). Evidence for a consistent change in the half way radius of the optical potential between  $^{116}\text{Sn}$  and  $^{120}\text{Sn}$  has been presented by Robertson et al. [Rob 71] on the basis of  $^{16,18}\text{O}$  elastic scattering studies.

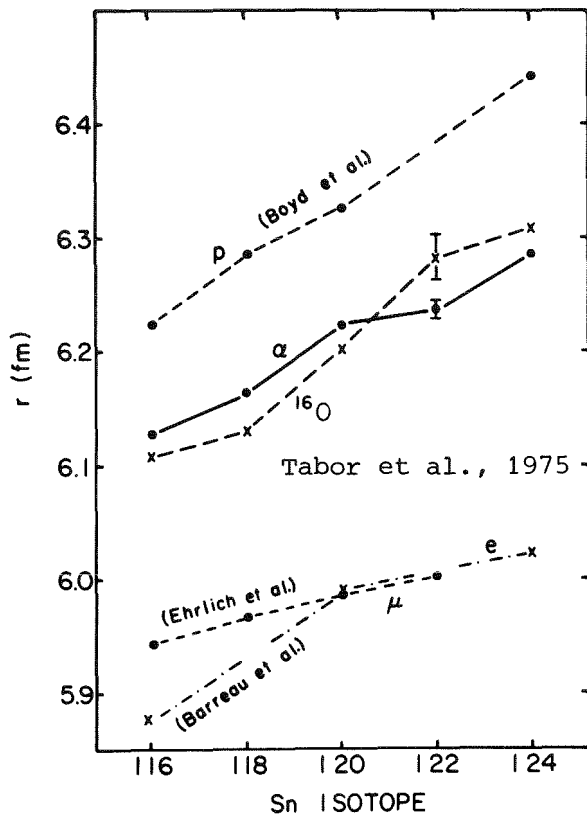


Fig.12: Size measurements of the tin isotopes by  $\alpha$ -particle and  $^{16}\text{O}$  scattering [Tab 75] as compared to results of proton scattering [Boy 71], of electron scattering [Ehr 68] and of muonic X-ray shifts [Ba Bel 67]

Apart from any discussion in which way strong absorption and Rutherford radii can be related to the nuclear density distribution they seem to be suitable to study the relative surface behavior of isotopes: isotopic differences in matter sizes of nuclei. The observed variations  $\Delta r_B$  e.g. in the case of the stable Sn and Ca isotopes prove to be different from the appreciably smaller variation of the charge distribution size within an isotopic series. This may be an effect of adding neutrons thus increasing the matter distributions by an amount which is larger than the increment in the proton distributions.

If the folding model representation for the interaction potential is valid, and if  $V_{\text{eff}}$  is known, then, in principle, one can determine the nuclear density distribution  $\rho_m(r)$  of the target nucleus, once the potential has been determined experimentally. This view has been taken in several recent studies [Ba Li 74, Sum 74, Ja Ro 76] which convert phenomenological optical potential - in that region where it is most reliably determined - into nuclear matter distribution information. Fig. 11 presents results of such a procedure fitting the magnitude and fall off rate of the surface potentials [Sum 74]. But deducing a value

of the rms radius implies a further step in assuming a particular form of  $\rho_m(r)$ , and the resulting value may be rather accidental and dependent on how appropriate the chosen form is.

The same statements holds for various other results compiled in tab.2. Here quoting a value of the rms radius involves necessarily a fairly large range of extrapolation of  $\rho_m(r)$  into the nuclear interior.

Though the low density situation of  $\alpha$  particle scattering seems to justify the simplest form of the folding model, there are some uncertainties since the influence of the imaginary part is not unimportant and affects some details of the information extracted [Ja Ro 76].

It may be of some interest to see in which way the folded potential resulting from the studies of elastic  $\alpha$ -particle scattering at 104 MeV [Gi Re 76] reproduces the barrier height and the Rutherford radius obtained from low energy scattering. As fig. 13 demonstrates there is surprisingly good agreement for the total potential ( $U_p + U_n + V_c$ ). Consideration of the different parts ( $U_p, U_n$ ) generated by the proton and neutron distribution, respectively, supports the preponderance of neutrons at the surface.

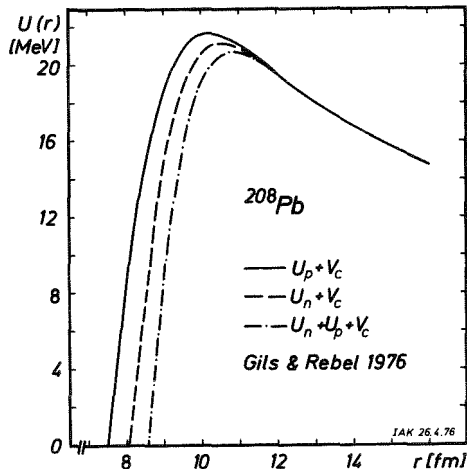


Fig. 13: Various parts of the folded potential resulting from 104 MeV  $\alpha$ -particle scattering by  $^{208}\text{Pb}$  as compared (Rutherford radius and barrier height) to low energy results [Gol 70, Ba Li 74] and to microscopic calculations [Ja Ro 76]

Values of the Rutherford radius  $r_R$  and the barrier height  $V_b$

Reference	$V_b$ [MeV]	$r_R$ [fm]
Goldring et al. [Gol 70]	20.42	10.9
Barnett & Lilley [Ba Li 74]	20.49	10.9
Analysis of Jackson & Rhoades - Brown : Different sets for $V_{eff}$	20.60	10.8
	20.33	11.0
	20.56	11.0
Gils & Rebel [Gi 76]		
$U_p + V_c$	21.7	10.2
$U_n + V_c$	21.2	10.5
$U_p + U_n + V_c$	20.7	10.8

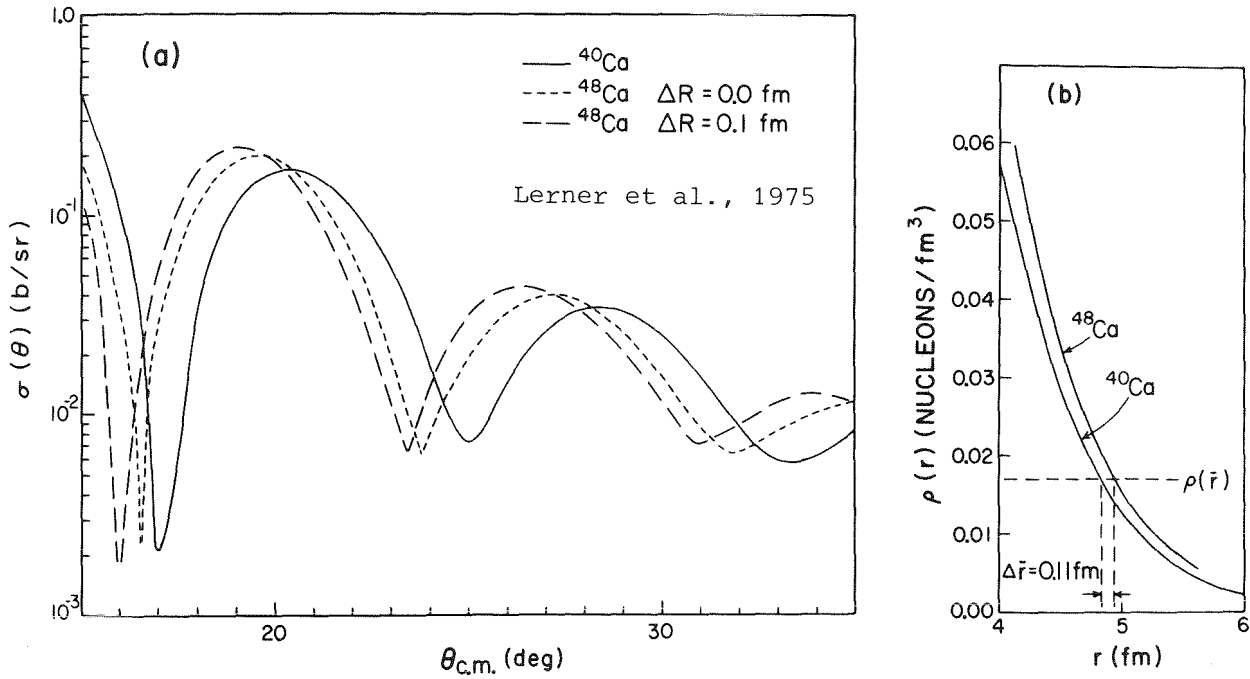


Fig. 14: (a) Calculated differential cross sections for 79 MeV  $\alpha$ -particle scattering with different assumed values  $\Delta R = \langle r^2 \rangle_{48}^{1/2} - \langle r^2 \rangle_{40}^{1/2}$   
 (b) Surface region for  $^{40,48}\text{Ca}$  in the surface region with the assumption  $\Delta R = 0$ . The radius  $\bar{r}$  is defined by the condition  $\rho(\bar{r}) = 0.017$  nucleons/ $\text{fm}^3$ .  
 (From Lern 75)

On the basis of the folding model approach we are able to clarify the meaning of the various interaction radii and of their differences in terms of the nuclear density distributions. In the past there has been some confusion attributing strong absorption radii differences to rms radii differences of the matter distribution. As noted in the context with recent  $\alpha$ -particle scattering studies of  $^{48}\text{Ca}$ - $^{40}\text{Ca}$  differences [Lern 75] a distinct shift in the diffraction pattern of the cross sections and a finite difference in the diffraction (strong absorption) radii are expected even for identical rms radii of the two isotopes compared (see fig. 19). This is due to different normalization of the density distributions of two different nuclei. Obviously differences in the diffraction and the Rutherford radii reflect density differences at certain points of the surface, not necessarily implying a finite rms radii difference. For this reason a comparison of trends of  $r_B$  with trends of rms (or equivalent uniform) charge radii seems not to be very conclusive.

### 3.4 Relative sizes of $^{40,48}\text{Ca}$ and neutron-proton rms radii differences of $^{48}\text{Ca}$

An illustrative example of the methodical concepts involved in using particle scattering experiments as a tool for investigating nuclear matter distributions originates from the problem of the relative sizes of  $^{40,48}\text{Ca}$  and the neutron-proton rms-radii differences of  $^{48}\text{Ca}$ . The information presently available is compiled in tab. 5. Recently the scattering of 79 MeV  $\alpha$ -particles from  $^{40,48}\text{Ca}$  has been measured with high relative accuracy and analyzed on the basis of a folding model [Lern 75]. The results for the difference between the  $^{40,48}\text{Ca}$  rms matter radii and for a possible neutron "halo" of  $^{48}\text{Ca}$  appear significantly smaller than results from comparable other studies including the Hartree Fock predictions. While there are arguments which may remove the discrepancies to diffraction or standard optical model analyses there is an apparent disagreement with high energy proton scattering results [Ahm 75]. In both cases the scattering from  $^{40}\text{Ca}$  is excellently described with  $\rho_n = \rho_p$ ,  $\rho_p(r)$  obtained from electron scattering so that the contradicting results, in the case of 1 GeV proton scattering by  $^{48}\text{Ca}$  requiring the neutron distribution  $\rho_n$  different from the proton distribution  $\rho_p$  (see fig.15), cannot be easily understood as a systematic defect of one of the reaction models used. It may be possible that the exchange effects (which are of minor importance at higher particle energies) are different for  $\alpha$ -scattering by  $^{48}\text{Ca}$  and  $^{40}\text{Ca}$  and lead effectively to the deduced  $^{40,48}\text{Ca}$  differences. Furthermore some sensitivities in treating the imaginary part may be masked. It should be mentioned that a recent analysis [Sum 74] of the real potential values near the strong absorption radii for 42 MeV  $\alpha$ -particles yields slopes of the matter distributions of  $^{40}\text{Ca}$  and  $^{48}\text{Ca}$  (see fig. 11) nearly identical to Negele's HF prediction [Neg 70]. Extrapolating the low density tails into the nuclear interior in terms of Fermi distributions larger  $^{40,48}\text{Ca}$  and neutron-proton differences of  $^{48}\text{Ca}$  are suggested ( $\langle r^2 \rangle_{48}^{1/2} - \langle r^2 \rangle_{40}^{1/2} \approx 0.25$  fm).

Method	$\langle r^2 \rangle_{48}^{1/2} - \langle r^2 \rangle_{40}^{1/2}$ [fm]	$\Delta r$ ( $^{48}\text{Ca}$ )	$\Delta R_{\text{Pot}}$	Definition of $R_{\text{Pot}}$	Reference
$\alpha$ -scattering 166 MeV	0.21±0.07	0.38±0.12			Tat72 - Bri72
79 MeV	0.05±0.04	0.03±0.03	0.18±0.04	Diffraction radius	Lern 75
42 MeV			0.11-0.25	Strong absorpt rad.	Fern70-Sum74
31 MeV			0.15	Radius parameter of Saxon-Woods pot.	Bern 69 a
$^{16}\text{O}$ -scattering 20-40 MeV			0.41±0.01	Rutherford radius	Ber 71
p-scattering 10.8-16.3 MeV	0.22±0.09	0.39±0.10		rms radius of the optical potential	Lom72
25-40 MeV			0.15	Radius parameter of Saxon-Woods pot.	Mag 70
1.04 GeV	≈ 0.15	0.24			Ahm75
Coulomb displacement energy		0.06			No Sch69
Hartree Fock prediction	0.190	0.227			Neg 70
Average of various HF predictions	0.17±0.03	0.18±0.04			(Lern 75)
Electron scattering	0.012				Bert 72

Tab. 5:  $^{48,40}\text{Ca}$  density and optical potential differences and  
neutron-proton rms-radii differences  $\Delta r$  of  $^{48}\text{Ca}$

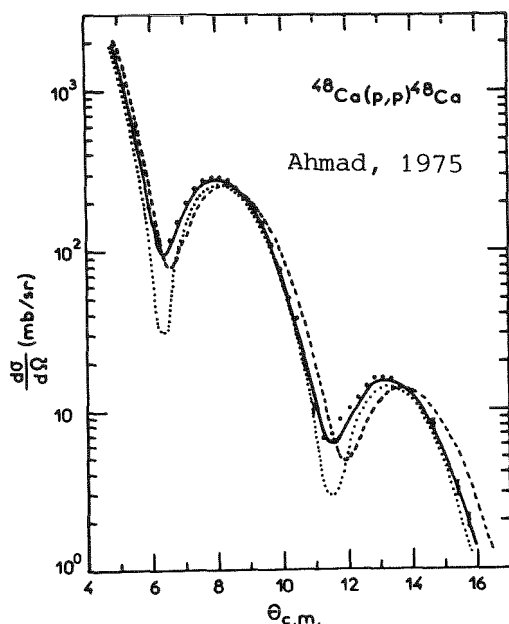


Fig. 15: Elastic differential cross sections of 1 GeV proton scattering from  $^{48}\text{Ca}$  |Ahm 75| - Experimental data are taken from the Leningrad group |Alk 72|  
 -----  $\rho_n = \rho_p$       ———  $\rho_n \neq \rho_p$   
 ..... without Coulomb scattering

#### 4. INELASTIC SCATTERING

##### 4.1 Deformed folding model approach

In order to refine the averaging "time exposures" in elastic scattering (in the sense of Baranger and Sorensen in Scientific American |BaSo 69|) we have to take snap shots by inelastic experiments. For nuclear particle scattering the most usual method used for determination of nuclear shapes is based on the extended optical model. In the framework of the collective model various low-lying excited states of nuclei are pictured as corresponding to shape vibrations or rotation. Consequently, the phenomenological description of these types of nuclear excitations is based on the assumption that the optical potential follows the static or dynamic deformation and becomes nonspherical. This is formulated by an adequate parametrization of the angular dependence of the interaction potential value, e.g. by the usual expansion of the radius parameter

$$R = R_0 \left( 1 + \sum_{1m} \alpha_{1m} Y_{1m}(\theta, \phi) \right) \quad (4.11)$$

defining the collective coordinates and providing a coupling whereby the projectiles could be inelastically scattered and excite collective states.

It is well known that such an approach has been very successful in describing the measured cross sections and angular distributions. The analysis extracts the coupling strengths: matrix elements of the transition operators which are built up by the collective coordinates and called "*deformation parameters*". It should be noted that we are interested not only in the absolute values of these matrix elements but also in their relative phases. For example, in the case of a permanent deformation the sign of the intrinsic quadrupole deformation parameter characterizes the nuclear shape as being prolate or oblate.

Extensive inelastic particle scattering studies in the past years have revealed that the differential cross sections carefully measured inform also on such details: signs of intrinsic deformation [Re 72a], deviation of axial symmetry [Gi 75] and hexadecapole components of the deformation [Hen 68, Swi 69, Re 71]. This information is due to the pronounced interference of single and higher order excitation processes which influence the observed diffraction pattern in a typical manner and which can be analyzed by a coupled channel procedure taking account of all important coupling via intermediate states.

Similar to the case of elastic scattering however the traditional description deriving the coupling potentials from a phenomenologically deformed interaction is not very satisfactory. It is far from obvious that the deformation of the optical potential should be identified with the deformation of the nucleus. Obviously, large projectiles - composite particles for which the range of the appropriate nucleon-projectile effective interaction is much greater than that of nucleon-nucleon - average over a large volume of the nucleus and see a smaller deformation. Such arguments suggest an extension of the folding model approach to inelastic scattering.

In so-called microscopic descriptions of inelastic scattering the coupling potentials  $U_{nn'}$  (form factors) for the nuclear excitation are generated by folding the effective interaction into the transition densities

$$\begin{aligned} \rho_{nn'}(\vec{r}) &= \langle n' | \sum_{i=1} \delta(\vec{r} - \vec{r}_i) | n \rangle & (4.12) \\ &= \sum \int \phi_{n'}^*(\vec{r}_1 \dots \vec{r}_A) \phi_n(\vec{r}_1 \dots \vec{r}_A) d^3 r_1 \dots d^3 r_{i-1} dr^3_{i+1} \dots d^3 r_A \end{aligned}$$

$$U_{nn'}(\vec{r}_\alpha) = \int \rho_{nn'}(\vec{r}) v_{\text{eff}}(\vec{r}, \vec{r}_\alpha) d^3 r = \sum_{LM} F_{LM}(r_\alpha) \cdot Y_{LM}(\hat{r}_\alpha) \quad (4.13)$$

where  $F_{LM}^{\alpha}(r_{\alpha})$  are the form factors of the (L,M)-pole-transition. This is obviously in analogy to the folding formula for elastic scattering. The ground state nuclear matter distribution  $\rho_m$  is replaced by the transition density which depends on the nuclear wave functions for the initial and final target nucleus states.

The natural application of the folding model to inelastic scattering from collective states and a reformulation of the extended optical model consists in deriving the transition densities of from *phenomenologically deformed matter distributions*. Such a semimicroscopic approach is a straight forward generalization of the corresponding procedure for elastic scattering. Following the critique of the extended optical model procedure [Ed Si 71, Ra Sp 71] it has been applied successfully to  $\alpha$ -particle and  ${}^3\text{He}$  scattering at higher energies ( $> 50$  MeV) [Re Sch73, Re 74a, Re 74b, Mac 73, Mac Ta 74, Gi 74, Mac Sw 75] where an increased sensitivity to size and shape parameters is observed and where exchange effects are expected to be of reduced importance.

In contrast to earlier DWBA-analyses we apply in the following examples the microscopic or semimicroscopic approach to both elastic and inelastic scattering in which the same effective interaction describes both processes. Obviously, especially for coupled channel analyses which handle elastic and inelastic scattering on equal footing this is more satisfactory and consistent.

In  $\alpha$ -particle scattering virtual transitions to intermediate states are known to be important. Thus, since a priori the folding model does not explicitly include the effects of virtual transitions the calculated spherical potential should be strictly understood as the spherical potential used in a coupled channel calculation rather than the potential required for fitting the elastic data when coupling is neglected.

We illustrate this approach by results of 104 MeV  $\alpha$ -particle scattering on  ${}^{56}\text{Fe}$ . In essence, the procedure consists in an application of the collective model - whatever the specific form may be - to the density distribution  $\rho_m$  of the integrand of the folding formula rather than to the optical potential. For technical details of deriving the coupling potentials we refer to original papers, especially to the appendix of the paper of Rebel et al. [Re 74a].

We start with a rotational model description of  ${}^{56}\text{Fe}(\alpha, \alpha') {}^{56}\text{Fe}$ .

The level positions and E2 properties of  ${}^{56}\text{Fe}$  are characteristic of an almost pure prolate rotator. The experimental  $B(E2; 0^+ \rightarrow 2_1^+)$ ,  $B(E2; 2_1^+ \rightarrow 4_1^+)$  and  $Q_2^+$ -values [Les 72] correspond to intrinsic quadrupole moments of  $98 \pm 1$ ,  $99 \pm 20$  and  $87 \pm 20$  efm<sup>2</sup>, respectively, derived on the basis of a symmetric rotator model. But they are also consistent with  $Q_0 = 102$  efm<sup>2</sup> and  $\gamma = 20^\circ$  in the asymmetric rotator model. Davydov and Chaban [Da Ch60] explained the level scheme of  ${}^{56}\text{Fe}$  in the framework of an asymmetric rotator model with  $\beta$ -vibrations resulting in  $\gamma = 17^\circ$  and a softness  $\mu = 0.61$ .

Fig. 16 compares the results of the extended optical model (Saxon-Woods potential with parameter values taken from a coupled channel calculation fit of the cross sections) to those of the folding model using a deformed nuclear density distribution of Fermi type. Of course, the main effect of the folding is a correction due to the finite size of the probe represented by the finite range of  $V_{\text{eff}}$ , and this is reflected by different values of the deformation parameters.

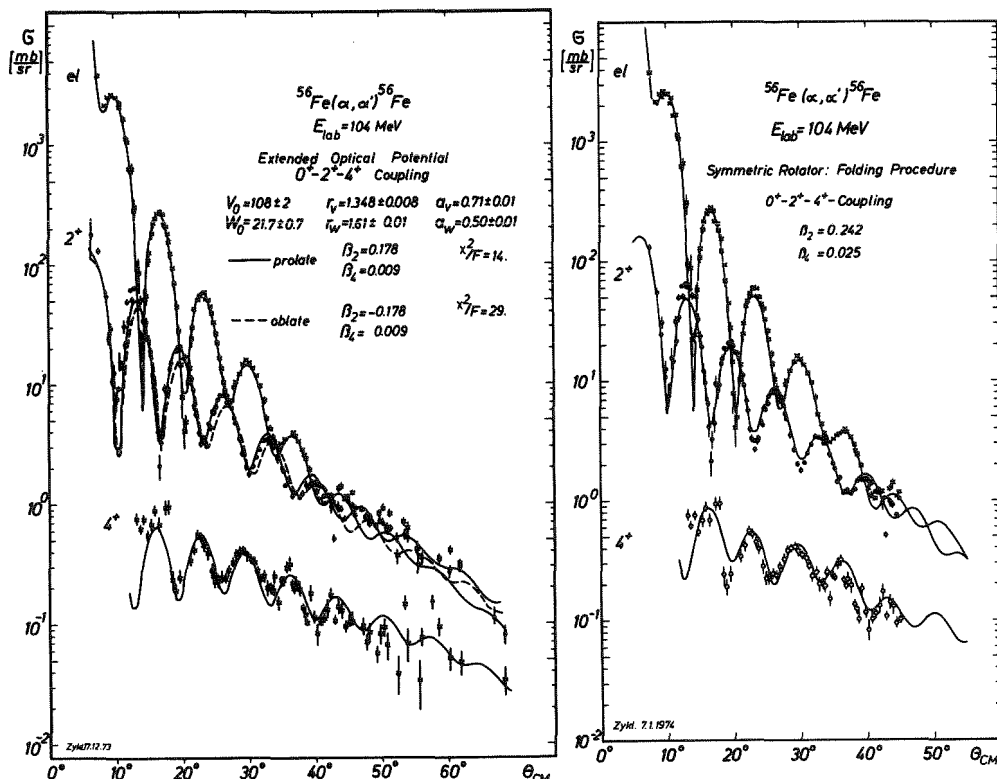


Fig. 16: Coupled channel analysis of the scattering of 104 MeV  $\alpha$ -particles from  $^{56}\text{Fe}$  on this basis of the rotational model |Gi 74|

The value of  $\beta_2 = 0.24$  of the underlying Fermi distribution corresponds to an intrinsic quadrupole moment which is in excellent agreement with the electromagnetic results. The prolate-oblate effects |Re 72a| are significant and give evidence for prolate deformation of  $^{56}\text{Fe}$  - in agreement with Coulomb excitation |Les 72|.

Hendrie |Hen 73a| has worked out a correction procedure based on a pure geometrical consideration assuming a spherical projectile interacting with a deformed nucleus only at their mutual sharply defined edges. With an  $\alpha$ -particle size of  $\Delta=1.6$  fm and a sharp edge size of  $1.2 \cdot A^{1/3}$  for  $^{56}\text{Fe}$  the value of  $\beta_2=0.24$  would correspond to the potential deformation  $\beta_2^{\text{pot}} \approx 0.18$ .

Tab. 6 compiles some results for nuclei of the 1f-2p-shell and compares with results of electron scattering and Coulomb excitation. Of course

the  $\alpha$ -particle scattering results are model-dependent. But in the framework of these specific collective models suggested by spectroscopic findings  $\alpha$ -particle scattering provides detailed information, for example, on the asymmetry of the deformation ( $^{48}\text{Ti}$ ,  $^{56}\text{Fe}$ ) or on hexadecapole deformations [Re Sch 73]. This table demonstrates the general agreement of the deformed folding model with electromagnetic results in cases where agreement should be expected. This is an empirical result remarkable in regard of the considerable uncertainties of such an approach.

The experimental cross sections determine the multipole moments (in addition to the rms radius) much better than the parameters of the adopted functional form of  $\rho_m(r)$ , in particular than the half way radius  $c_m$  and the diffuseness  $a_m$  of a Fermi shape [Mack 74, Gi Re 75b]. As already indicated for elastic scattering regarding the rms radius the values of the two parameters  $c_m$  and  $a_m$  can scatter over a fairly large acceptable range combined in such a way that the rms radius is reproduced with nearly stable value. For the case of  $\alpha$ -particle scattering from  $^{56}\text{Fe}$  such parameter correlations (including the deformation parameter) and the sensitivities of the measured cross sections are illustrated in fig. 17 by presenting contour plots of the  $\chi^2$ -values (goodness of fit) in various parameter planes through the minimum values  $\chi_{\min}^2$ . The various curves are sections through the  $\chi_{\min}^2$  point envelopped by the hypersurface  $\chi^2 = 2 \cdot \chi_{\min}^2$  in the multidimensional parameter space. While the deformation parameters affect the rms radius less, they distinctly influence the  $Q_{20}$  value which is rather well defined, especially by the inelastic cross sections.

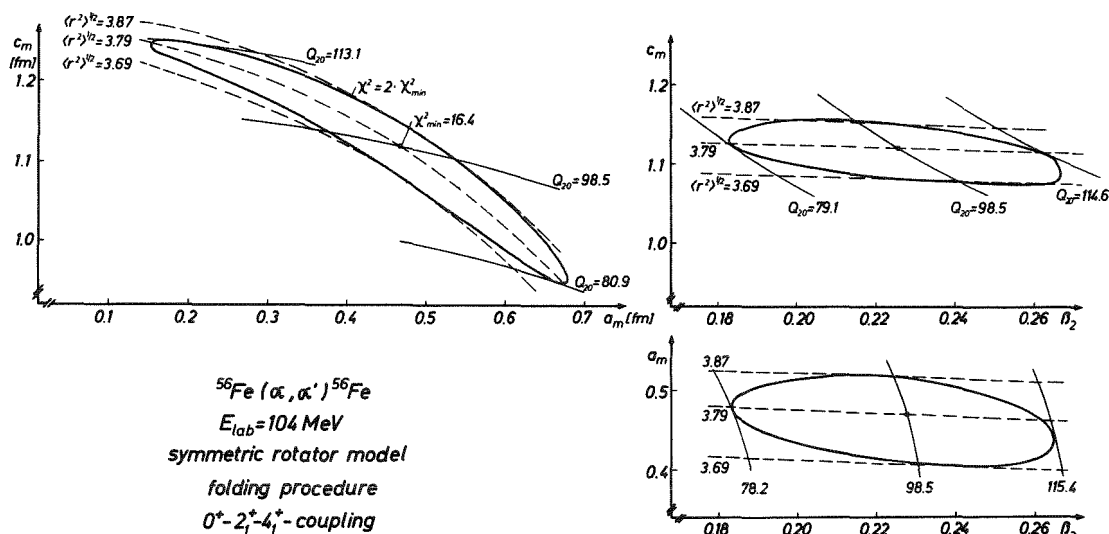


Fig. 17: Example  $^{56}\text{Fe}(\alpha, \alpha')^{56}\text{Fe}$ : Contour plots of the values  $\chi^2 = 2 \cdot \chi_{\min}^2$  in various parameter planes through the minimum value  $\chi_{\min}^2$

Nuclide	46Ti	48Ti	50Ti	56Fe	
$\langle r^2 \rangle^{1/2}$ [fm]	3.64±0.15	3.56±0.04	3.60±0.07	3.75±0.06	3.82±0.06
$B(E2, 0^+ \rightarrow 2^+)$ [e <sup>2</sup> fm <sup>4</sup> ]	874±56	763±40	280±26	1009±62	1047±60
$Q_2$ [e fm <sup>2</sup> ]	-27±1	-19±1	—	-29±1	-29±1
$\xi$	—	≈ 24°	—	—	≈ 19°
Analysis	Symmetric Rotator	Triaxial Rotator	Anharmonic Vibrator	Symmetric Rotator	Triaxial Rotator
$\langle r^2 \rangle^{1/2}$ [fm]	3.55±0.04			3.74±0.07	
$B(E2, 0^+ \rightarrow 2^+)$ [e <sup>2</sup> fm <sup>4</sup> ]	970±70	690±60	330±30	970±20	
$Q_2$ [e fm <sup>2</sup> ]	-19±10	-13.5±8.8	-2±9	-24.9±5.8	

Tab. 6: Folding model results for scattering of 104 MeV  $\alpha$ -particles from 1f-2p-shell nuclei [Re 74a, Gi 74, Gi 75] as compared to electromagnetic results.

#### 4.2 Prolate-oblate effects and $(\alpha, \alpha' \gamma)$ angular correlation measurements

The pronounced interference of single and higher order excitation process which influences the observed distinct diffraction pattern of the differential cross sections, in particular of  $\alpha$ -particle scattering, allows a sensitive coupled channel analysis discriminating prolate and oblate intrinsic deformations of nuclei [Re 72a, Re 72b]. The effects observed (small shifts of the diffraction maxima and changes of the oscillation period in the  $2^+$  cross section as compared to the elastic angular distribution) are qualitatively predicted by simple diffraction models including second order terms in the deformation parameters [In Sh 67, Go Yu 71, Re 72a]. Recent studies show that the sensitivity to the sign of the intrinsic deformation is considerably increased when observing the  $(\alpha, \alpha' \gamma)$  angular correlation.

Similar to experiments with polarized projectiles particle-angular correlation studies provide more insight into the reaction mechanism than differential cross section measurements. From  $(\alpha, \alpha_1 \gamma)$  angular correlation measurements on even-even nuclei the reaction amplitude  $X_m$  referring to different magnetic substates of the residual excited  $2_1^+$  state can be determined separately [Wag 73]. In the context with more refined studies of the folding model  $^{24}\text{Mg}(\alpha, \alpha' \gamma)$  angular correlation measurements have been performed with 104 MeV  $\alpha$ -particles [Eyr 76]. Fig. 18 which displays in the lower part the squared reaction amplitude  $|X_0|^2$  (the z-axis is chosen perpendicular to the scattering plane) demonstrates the predictive power of the folding model.

The theoretical curves result from coupled channel calculations using electron scattering results for the parameters of a deformed nuclear distribution of  $^{24}\text{Mg}$  [Na To 72].

The upper part of fig. 18 shows the correlation parameter  $C \propto |x_2| \cdot x_{-2} \cdot (d\sigma/d\Omega)^{-1}$  as function of the particle scattering angle for positive and negative intrinsic quadrupole deformation of  $^{24}\text{Mg}$ , respectively. The experimental data favour clearly prolate shape.

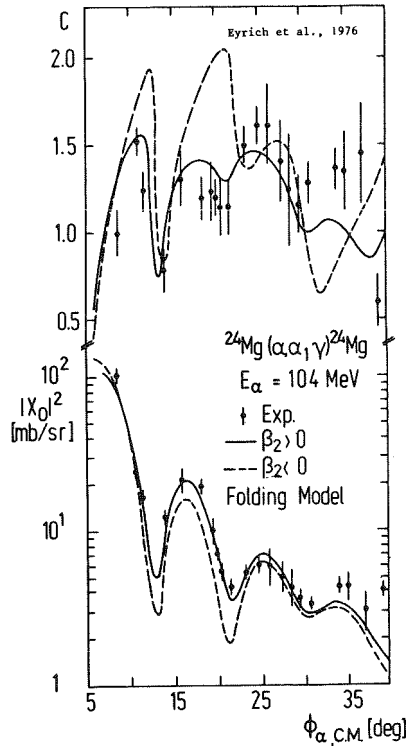


Fig. 18: 104 MeV  $\alpha$ -particle scattering from  $^{24}\text{Mg}$ : Substate cross section  $|X_0|^2$  and correlation parameter  $C$  (in  $(\alpha, \alpha'\gamma)$  measurements experimentally determined by fitting the in plane correlation function  $W(\phi_\gamma) = A + C \sin^2(2(\phi_\gamma - \phi_0))$

#### 4.3 Generalized collective model and $\alpha$ -particle scattering

The collective models used hitherto are relatively simple and limiting cases for the collective behavior of nuclei. In particular, nuclei of the 1f-2p shell exhibit features characteristic of soft nuclei. The properties of the low-lying levels indicate collective features intermediate between harmonic vibrations and rigid rotations [Cli 71]. In such transitional cases we need a more general and flexible description - generalized collective model - as formulated e.g. by Gneuß and Greiner [Gneu Gr 71]. As for any other collective Hamiltonian we have to determine several mass- and stiffness parameters which, in principle, may be related to a microscopic description of the collective motion. We used, however, a rather phenomenological procedure in determining these parameters by fitting the experimental level schemes

and  $B(E2; 0^+ \rightarrow 2_1^+)$  transition probabilities. Such a procedure has been proved to be very successful in a range of cases [Re Ha 73, Hab 74]. The collective behavior of the nuclei is displayed by their so called collective energy surfaces. They represent the potential energy of the nuclei as function of the shape parameters. With restriction to quadrupole deformations all possible shapes can be described by the two wellknown deformation and asymmetry parameters  $\beta$  and  $\gamma$ . Fig. 19 shows the collective energy surfaces of  $^{48}\text{Ti}$  and  $^{56}\text{Fe}$  given as contour maps on the  $\beta$ - $\gamma$ -plane. Symmetry properties confine the considerations to a sector  $0^\circ < \gamma < 60^\circ$ . In this sector the potential energy surfaces and the collective wave functions are defined. The shadowed contours indicate the level of the ground states and the range of the zero-point-oscillations. This may be taken as a measure of the softness of these nuclei:  $^{48}\text{Ti}$ , a  $\beta$ -soft nucleus with asymmetric deformation,  $^{56}\text{Fe}$  somewhat more complicated exhibiting a second minimum, yet in the zero-point oscillations.

In view of the considerable importance of the collective energy surfaces with regard on heavy ion scattering, nuclear fission etc. it is certainly interesting to check such calculations by  $\alpha$ -particle scattering.

Formally, the generalized collective model is an anharmonic vibrational model of high order\*. This implies that

1. the matrix elements of second and higher orders of the collective coordinates contribute significantly
2. the values of the matrix elements are strongly dependent on the connected states in rather complex relations.

The matrix elements for the  $(\alpha, \alpha')$ -scattering calculations are obtained directly by the solutions of the collective Hamilton. The radial behavior of the density distribution can be taken from elastic or electron scattering, and as also the effective interaction is fixed, we have not to adjust any parameters.

The sensitivity of the scattering cross sections to higher order matrix elements is shown in fig. 20 and demonstrates that 100 MeV

\*)

Requiring volume conservation and considering terms of higher order a monopole term  $\alpha_{00}$  has to be introduced into the expansion of the nuclear radius and induces additional coupling terms [Re 74b].

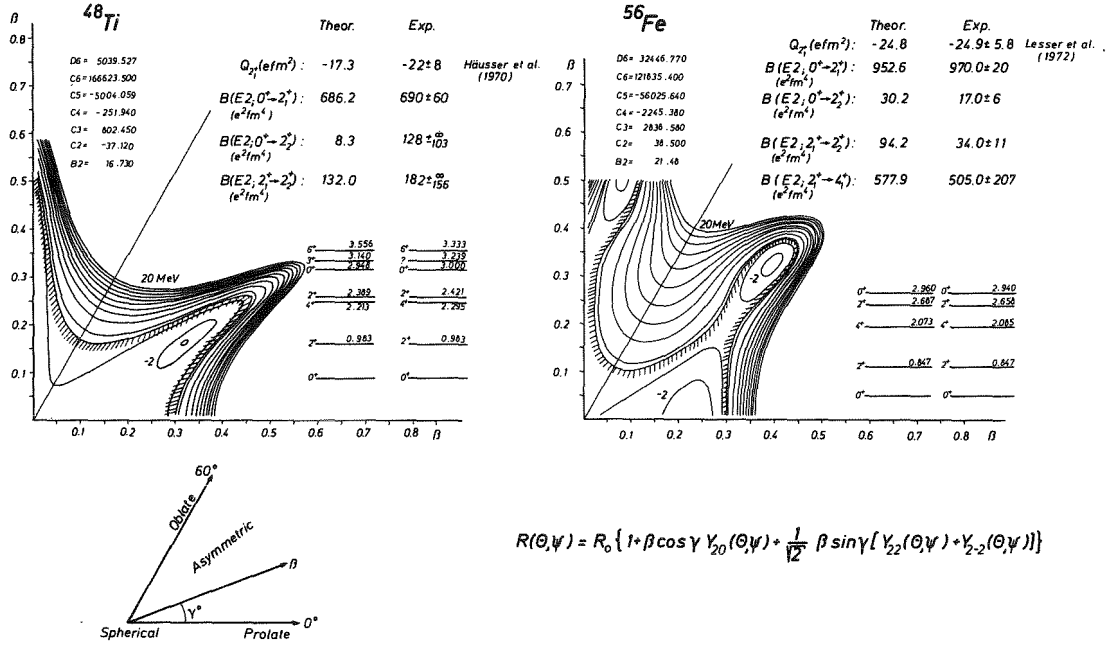


Fig. 19: Collective energy surfaces of <sup>48</sup>Ti and <sup>56</sup>Fe resulting from an analysis of level spectra and E2 properties in the framework of the model of Gneuß and Greiner [Re 74b]

$\alpha$ -particles are able to "see" the rather complicated nuclear shapes represented by the collective energy surfaces in fig. 19. Fig. 20 demonstrates the excellent agreement of  $\alpha$ -particle scattering with the generalized collective model. The imperfectness for the  $2^+_{-2}$ -cross section may indicate the presence of an unknown admixture to the  $2^+_{-2}$ -amplitude (e.g. coupling of two quasiparticle states neglected in the generalized collective model). This assumption is not unreasonable for a level of 2.7 MeV above the ground state. In view of the extreme sensitivity of the  $\alpha$ -particle cross sections to such additional components there is no serious objection against the generalized collective model description of the low lying states.

We may conclude that the generalized collective model - even if we would hesitate to take it too literally in the form indicated here - proves to be an excellent basis for a unified description of level scheme, E2-properties and  $\alpha$ -particle scattering. Scattering of  $\alpha$ -parti-

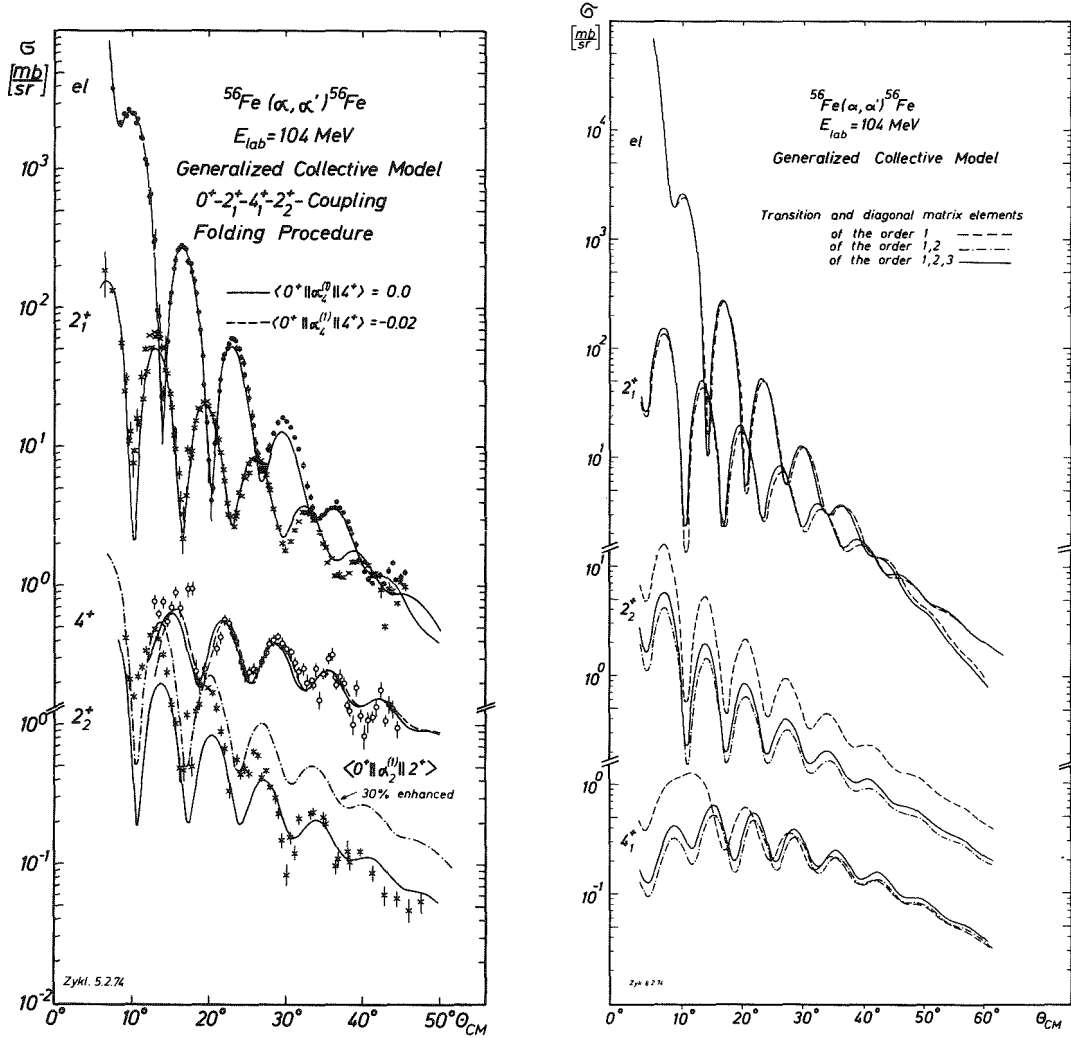


Fig. 20 Generalized collective model description of  $^{56}\text{Fe}(\alpha, \alpha')^{56}\text{Fe}$  at  $E_{\alpha} = 104 \text{ MeV}$  [Re 74b]

- a) Coupled channel predictions and experimental cross sections
- b) Theoretical cross sections calculated by including different orders of the transition matrix elements.

cles is sensitive enough to reveal more complicated collective features and to draw attention to necessary improvements of the current structure models.

#### 4.4 Hexadecapole deformation in nuclei

Since Hendrie et al. [Hen 68] have clearly demonstrated the possibility of accurate determinations of hexadecapole deformation of rare earth nuclei by inelastic  $\alpha$ -particle scattering at 50 MeV, higher multipole deformation is no more experimental "terra incognita". In addition to the electromagnetic information provided by inelastic electron scattering [Bert 72a] and Coulomb excitation experiments [see Dia 73, Pe Smi 73] inelastic scattering of strongly interacting projectiles well above the Coulomb barrier - of unpolarized and polarized protons,  $^3\text{He}$ - and  $\alpha$ -particles - has been proven to be a reliable and comfortable tool to measure magnitudes and signs of higher order deformations, in some cases with surprisingly high sensitivity. The acquired data on deformation parameters associated with the nuclear potential pose again the question concerning the relationship between potential shape and shape of the nuclear matter distribution. Ignoring this question a puzzling discrepancy had become apparent for  $\beta_4$  deformation parameters observed in (p,p'), (e,e'), ( $\alpha,\alpha'$ ) and ( $\tau,\tau'$ ) experiments for 2s-1d shell nuclei [Swi 69, Hor 71, Re 71, Swi 74]. The values of the deformation parameters found by ( $\alpha,\alpha'$ ) scattering proved to be significantly smaller than the values from (p,p') and (e,e') experiments. Similar tendencies have become apparent for the multipole deformation parameters of rare earth and actinide nuclei for which substantial equilibrium deformation up to L=6 have been experimentally demonstrated [Mos 71, Hen 73b, Bem 73, Dav 76]. A systematic comparison of charge deformation and the deformation of the optical potentials reveals significant deviations increasing with the multipolarity and interpreted now to be differences between potential and nuclear shape. Indeed, applying a folding model description the reanalyses of the ( $\alpha,\alpha'$ ) and ( $\tau,\tau'$ ) scattering from  $^{20}\text{Ne}$  and  $^{28}\text{Si}$  have been able to remove the main part of the previously observed discrepancies [Re Sch 73, Mac Sw 75, Swi 76].

The experimental information on multipole deformation of the actinide nuclei is some what obscured by deficiencies of the analyses performed. It has been demonstrated by recent calculations using realistic charge distributions that details of the target nucleus charge distribution influence the extracted values of  $\beta_L$  [Re Ge 76] at energies not far away from the Coulomb barrier.

Although such a consideration of higher multipole deformation strongly supports the relevance of the folding approach it should be noted that

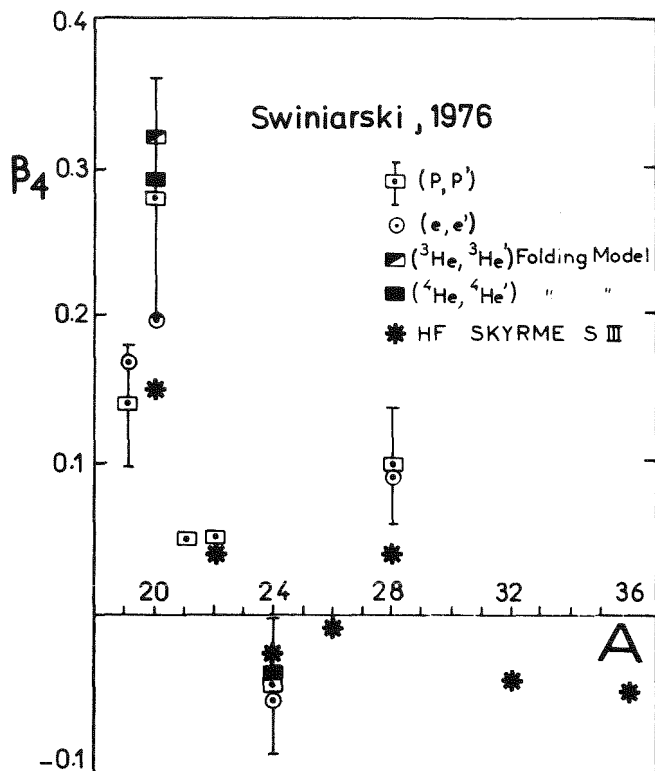


Fig. 21: Hexadecapole deformation of 2s-1d shell nuclei. Results of various analyses of experimental scattering data as compared to theoretical predictions | Swi 76 |

the uncertainties entering into explicit folding model calculations, in particular due to exchange effects, are most likely more important just for the higher multipole components in nuclear shape. In order to track out some uncertainties in specifying the most adequate effective interaction, Mackintosh [Mac 76] has proposed the application of Satchler's theorem [Sat 72] which relates the moments of a folded potential to the moments of the nuclear density distribution by

$$\frac{\int U(\vec{r}_\alpha) r_\alpha^L Y_L^M(\hat{r}_\alpha) d^3 r_\alpha}{\int U(\vec{r}_\alpha) d^3 r_\alpha} = \frac{\int \rho_m(\vec{r}) r^L Y_L^M(\hat{r}) d^3 r}{\int \rho(\vec{r}) d^3 r} \quad (4.41)$$

This implies the following statement: *Provided that the true (experimentally unambiguously observed) interaction potential  $U(\vec{r}_\alpha)$  is really generated by the folding procedure we need not to know the detailed form of  $V_{eff}(\vec{r}, \vec{r}_\alpha)$  even in the case that the effective projectile-bound nucleon interaction is a rather complicated superposition of various components of different ranges. This seems to open a rather interesting and convenient way translating the empirical potential distribution into nuclear structure information, especially when considering higher multipole moments. Due to the  $r^L$  dependence of the integrands these moments, are mainly determined by the surface where the*

potential may be fairly well understood to be generated by folding. On the other hand consideration of volume integrals and potential rms radii casts doubt that such an assumption is valid in general [Re 76].

## 5. CONCLUSIONS

The real part of the optical model potential describing medium and intermediate energy nucleon and  $\alpha$ -particle scattering from nuclei is a possible source of information regarding sizes and shapes of nuclei. The selected examples presented here illustrate the various approaches and procedures in deriving relevant nuclear shape information from scattering experiments, and they may indicate the particular type of the information extracted, some limitations and uncertainties involved. In the process of doing so the investigations have established, at least on an empirical basis, considerable evidence of the relevance of a reaction model which is represented by the first term of a multiple scattering expansion of the optical potential and has prepared a way to the desired information on *radial shapes of nuclei*. A justified applicability of this simplified scattering model is connected with the extent to which the probing particle can escape the many body dynamics in the nucleus. Following this argument the strong absorption localizing the scattering process to the nuclear surface favors  $\alpha$ -particle scattering, even if the information provided must be considered to be confined to the surface, strictly. While the interpretation of medium energy nucleon scattering requires a more detailed understanding of various delicate sensitivities,  $\alpha$ -particle proves to be a rather uncomplicated tool since obviously only the gross structure of the effective interaction seems to be important and can be calibrated in well determined cases. The main uncertainties entering  $\alpha$ -particle scattering analyses arise from insufficiently known exchange effects which certainly influence inelastic scattering to a larger extent than elastic scattering, and from the imaginary part of the optical which is only phenomenologically accessible and may simulate effects not yet explored.

Alternatively, the most vicious tricks of the nuclear many body problem are also assumed to be controlled when increasing the incident energy of the probes. The group at Saturne is going particularly rigorously in this promising direction. In some points the present

analyses of high energy proton scattering seem still somewhat oversimplified as not all essential ingredients are clearly pinned down: spin part and the ratio of the real to imaginary part of the NN amplitude, and the influence of pair correlations. There are some certain aspects which seem to be less complicated in pion scattering although pion scattering appears to be presently in an earlier stage of development (and is excluded from this report without any further judgement as to value).

Proton and  $\alpha$ -particle mean free paths are expected to be different and the comparison can provide a sensitive test of the methods of analyses used to extract rms radii and other moments of the nuclear density distributions. In general we find surprisingly good agreement. Nevertheless despite of the fact that reasonable approaches lead to reasonable results much thinking should go in those effects which one does not yet control thus throwing a practicable bridge across the apparent gap between phenomenological efforts and a detailed microscopic theory.

*"Si les plats que je vous offre sont  
mal préparés, c'est moins la faute de  
mon cuisinier que celle de la chimie,  
qui est encore dans l'enfance."  
(La Rôtisserie de la reine Pédauque).*

*Anatole France*

## Acknowledgement

This report is intended to be an experimentalist's view of the sense and the current situation of scattering of strongly interacting projectiles providing information on nuclear matter distribution.

It is a pleasure to acknowledge illuminating conversations with P. Brix, H.J. Gils, K. Grotowski and G. Schatz. I am greatly indebted to all colleagues who have generously permitted the quotation or reproduction of their work. And I would especially thank Mrs. E. Kirste and Miss W. Nowatzke for responding to the challenge of producing this copy from my handwritten notes.

## References

- Ahm 75 I. Ahmad, Nucl. Phys. A247 (1975) 418
- Alla 73 B.W. Allardyce, C.J. Batty, D.J. Baugh, E. Friedman, G. Heymann, M.E. Cage, G.J. Pyle, G.T.A. Squier, A.S. Clough, D.F. Jackson, S. Murugesu, V. Rajaratnam, Nucl. Phys. A209 (1973) 1
- Alk 72 G.D. Alkhazov, G.M. Amalsky, S.L. Belostotsky, A.A. Vorobyov, O.M. Domchenkov, Yu.Y. Dotsenko and V.F. Starobubsky, Phys. L. 42B (1972) 121
- Alv 70 H. Alvensleben, U. Becker, W.K. Bertram, M. Chen, K.J. Cohen, T.M. Knasel, R. Marshall, D.J. Quinn, M. Rohde, G.H. Sanders, H. Schubel and S.C.C. Ting, Phys. Rev. L. 24 (1970) 792
- Au 68 E.M. Auerbach, H.M. Qureshi and M.M. Sternheim, Phys. Rev. L. 21 (1968) 169
- Au Lom 74 J.P. Auger and R. Lombard, Nuov. Cim. 21 (1974) 529
- Ba Bel 67 P. Barreau and J.B. Bellicard, Phys. L. 25B (1967) 470
- Bad 74 J. Badaway, Thèse 1974, Université de Paris-Sud Centre d'Orsay  
J. Badaway, B. Berthier, P. Charles, M. Dost, J. Gastebois, B. Fernandez and S.M. Lee (to be published)
- Ba Li 74 A.R. Barnett and J.S. Lilley, Phys. Rev. C9 (1974) 2010
- Bat 71 C.J. Batty, E. Friedman and D.F. Jackson, Nucl. Phys. A175 (1971) 1
- Bat Fri 71 C.J. Batty and E. Friedman, Phys. L. 34B (1971) 7
- Bat Fri 72 C.J. Batty and E. Friedman, Nucl. Phys. A179 (1972) 707
- Ba So 69 M. Baranger and R.A. Sorenson, Scientific American 221 (1969) 58
- Ba Wi 68 R.H. Bassel and C. Wilkin, Phys. Rev. 174 (1968) 1179
- Bem 73 C.E. Bemis, Jr., F.K. Mc Gowan, J.L.C. Ford, Jr., W.T. Milner, P.H. Stelson and R.L. Robinson, Phys. Rev. C8 (1973) 1466
- Ber 71 M.C. Bertin, S.L. Tabor, B.A. Watson, Y. Eisen and G. Goldring, Nucl. Phys. A167 (1971) 216
- Bern 69a A.M. Bernstein, M. Duffy and E.P. Lippincott, Phys. L. 30B (1969) 20
- Bern 69b A.M. Bernstein, Adv. Nucl. Phys. 3 (1969) 325, eds. M. Baranger and E. Vogt
- Bern 71 A.M. Bernstein and W.A. Seidler, Phys. L. 34B (1971) 569

- Bern 72 A.M. Bernstein and W.A. Seidler, Phys. L. 39B (1972) 583
- Ber Pa 76 A.M. Bernstein and C. Papanicolas, Contribution to the second Conference "Radial Shape of Nuclei", Cracow, 1976
- Bert 72a W. Bertozzi, T. Cooper, N. Ensslin, J. Heisenberg, S. Kowalski, M. Mills, S.P. Fivozinsky, J.W. Lightbody, Jr. and S. Penner, Phys. Rev. L. 28 (1972) 1711
- Bert 72b W. Bertozzi, J. Friar, J. Heisenberg and J.W. Negele, Phys. L. 41B (1972) 408
- Berti 73 R. Bertini, R. Beurtey, F. Brochard, G. Bruge, H. Catz, A. Chaumeaux, J.M. Durand, J.C. Faivre, J.M. Fontaine, D. Garreta, C. Gustafsson, D. Hendrie, F. Hibou, D. Legrand, J. Saudinos and J. Thirion, Phys. L. 45B (1973) 119
- Bli 69 R.J. Blin-Stoyle, Phys. L. 29B (1969) 12
- Boj 69 A.M. Borjarski, R. Diebold, S.D. Ecklund, G.E. Fischer, Y. Murata, B. Richter and M. Sands, Phys. Rev. L. 23 (1969) 1343
- Boy 71 R.N. Boyd, J. Fenton, M. Williams, T. Kruse and W. Savin, Nucl. Phys. A162 (1971) 497
- Boy Gr 68 R. Boyd and G.W. Greenlees, Phys. Rev. 176 (1968) 1394
- Bri 72 J. Brissaud, Y. Le Bornec, B. Tatischeff, L. Bimbot, M.K. Brussel and G. Duhamel, Nucl. Phys. A191 (1972) 145
- Bri Br 76 I. Brissaud and M.K. Brussel, Preprints 1976, Contribution to the second Conference "Radial Shape of Nuclei", Cracow 1976
- Bud 70 A. Budzanowski, A. Dudek, K. Grotowski and A. Strzalkowski, Phys. L. 32B (1970) 431
- Bug 73 W.M. Bugg, G.T. Condo, E.L. Hart, H.O. Cohn and R.D. Mc Cullock, Nucl. Phys. B64 (1973) 29 - Phys. Rev. L. 31 (1973) 475
- Ca Sp 72 X. Campi and D. Sprung, Nucl. Phys. A194 (1972) 401
- Cli 71 D. Cline, Proc. Colloq. on intermediate nuclei, Orsay, France 1971, UR-NSRL 59 (1972)
- Da Ch 60 A.S. Davydov and A.A. Chaban, Nucl. Phys. 20 (1960) 499
- Dav 76 P. David, W. Soyez, H. Essen, H.V. v. Geramb, Preprint 1976
- Dia 73 R.M. Diamond, Journ. Phys. Soc. Japan 34 Supp. (1973) 118
- Do Var 74 C.B. Dover and J.P. Vary, Proceedings of the Symposium on Classical and Quantum Mechanical Aspects of Heavy Ion Collisions, Heidelberg, Germany, Oct. 2-5, 1974
- Ed Sin 71 V.R.W. Edwards and B.C. Sinha, Phys. L. 37B (1971) 225
- Eis 72 Y. Eisen, R. Eisenstein, U. Smilansky and Z. Vager, Nucl. Phys. A195 (1972) 513
- Ehr 68 R.D. Ehrlich, Phys. Rev. 173 (1968) 1088
- Eu 76 H. Euteneuer, J. Friedrich and N. Voegler, Phys. Rev. L. 36 (1976) 129
- Eyr 76 W. Eyrich, A. Hofmann, U. Scheib, S. Schneider, F. Vogler and H. Rebel, Contribution to the second Conference "Radial Shape of Nuclei", Cracow 1976 - Phys. Rev. L. (submitted)
- Fern 70 B. Fernandez and J.S. Blair, Phys. Rev. C1 (1970) 523

- Fes 71 H. Feshbach, A. Gal and J. Hüfner, *Ann. Phys. N.Y.* 66 (1971) 20
- Fes Hü 70 H. Feshbach and J. Hüfner, *Ann. Phys. N.Y.* 56 (1970) 268
- Fran 72 V. Franco, *Phys. Rev.* C6 (1972) 748
- Fri 69 E. Friedman, *Phys. L.* 29B (1969) 213
- Fri 74 E. Friedman, *Phys. Rev.* C10 (1974) 2082
- Fro 68 R.F. Frosch, R. Hofstadter, J.S. Mc Carthy, G.K. Nöldeke, K.J. von Oostrum, M.R. Yearian, B.C. Clark, R. Herman and D.G. Ravenhall, *Phys. Rev.* 174 (1968) 1380
- Gi 74 H.J. Gils, H. Rebel and A. Ciocanel, *Rev. Roum. de Phys.* 19 (1974) 761
- Gi 75 H.J. Gils, H. Rebel, G. Nowicki, A. Ciocanel, D. Hartmann, H. Klewe-Nebenius and K. Wisshak, *Journ. Phys. G (Nucl. Phys.)* 1 (1975) 344
- Gi 75a H.J. Gils and H. Rebel, *KFK-Report* 2127 (1975)
- Gi 75b H.J. Gils and H. Rebel, *Z. Phys.* A274 (1975) 259
- Gi Re 76 H.J. Gils and H. Rebel, *Contribution to the Symposium on Nuclear Structure, Balatonfüred, Hungary, Sept. 1-7, 1975*, *Phys. Rev. C* (1976)
- Gla Ma 70 R.J. Glauber and G. Matthiae, *Nucl. Phys.* B21 (1970) 135
- Glau 59-69 R.J. Glauber, in *Lectures in Theoretical Physics*, ed. by E.W. Brittin et al., Vol. 1, (New York 1959) 315; *High Energy Physics and Nuclear Structure (Proceedings of the II International Conference, Rehovoth 1967)*, ed. by G. Alexander (Amsterdam 1967) - *High Energy Physics and Nuclear Structure (Proceedings of the III International Conference, Columbia 1969)*, ed. by S. Devons (New York 1970) 207
- Gneu Gr 71 G. Gneuß and W. Greiner, *Nucl. Phys.* A71 (1971) 449
- Gol 70 G. Goldring, M. Samuel, B.A. Watson, M.C. Bertin and S.L. Tabor, *Phys. L.* 32B (1970) 465
- Go Yu 71 V. Yu Gonchar and A.V. Yushkov, *Bull. Acad. of Sci. USSR, Phys. Ser.* 35 (1971) 558
- Green 68 G.W. Greenlees, G.J. Pyle and Y.C. Tang, *Phys. Rev.* 171 (1968) 1115
- Green 70a G.W. Greenlees, W. Makofske and G.J. Pyle, *Phys. Rev.* C1 (1970) 1145
- Green 70b G.W. Greenlees, V. Hnizdo, O. Karban, J. Lowe and W. Makofske, *Phys. Rev.* C2 (1970) 1063
- Hab 74 D. Habs, H. Klewe-Nebenius, K. Wisshak, R. Löhken, G. Nowicki and H. Rebel, *Z. Phys.* 267 (1974) 149
- Heis 69 J. Heisenberg, R. Hofstadter, J.S. Mc Carthy, J. Sick, B.C. Clark, R. Herman, D.G. Ravenhall, *Phys. Rev. L.* 23 (1969) 1402
- Hen 68 D.L. Hendrie, N.K. Glendenning, B.G. Harvey, O.N. Jarvis, H.H. Duhm, J. Saudinos and J. Mahoney, *Phys. L.* 26B (1968) 127
- Hen 73a D.L. Hendrie, *Phys. Rev. L.* 31 (1973) 478
- Hen 73b D.L. Hendrie, B.G. Harvey, J.R. Meriwether, J. Mahoney, J.-C. Faivre and D.G. Kovar, *Phys. Rev. L.* 30 (1973) 571
- Ho Wi 68 B. Holmquist and T. Wiedling, *Phys. L.* B27 (1968) 411
- Hor 71 Y. Horiawa, Y. Torizuka, A. Nakada, S. Mitsunobo, Y. Kojima and M. Kimura, *Phys. L.* 36B (1971) 9

- Hü Ma 72 J. Hüfner and C. Mahaux, Ann. Phys. (N.Y.) 73 (1972) 525
- In Sh 67 E.V. Inopin and A.V. Shebeko, JETP (Sov. Phys.) 24 (1967) 1189
- Ja Mo 68 D.F. Jackson and C.G. Morgan, Phys. Rev. 175 (1968) 1402
- Ja Ke 69 D.F. Jackson and V.K. Kumbhavi, Phys. Rev. 178 (1969) 1626
- Ja Ro 76 D.F. Jackson and M. Rhoades-Brown, Preprint 1976
- Ker 59 A.K. Kerman, H. McManus and R.M. Thaler, Ann. Phys. (N.Y.) 8 (1959) 551
- Khr 70 V.M. Khrastunov, N.G. Afanasyev, V.D. Afanasyev, I.S. Gukarov, A.S. Omelaenko, G.A. Savitsky, A.A. Khomich, N.G. Shevchenko, V.S. Romanov and N.V. Rusanova, Nucl. Phys. A146 (1970) 15
- Ki Ro 71 H.R. Kidwai and J.R. Rook, Nucl. Phys. A169 (1971) 417
- Ko Ma 69 O. Kofoed-Hansen and B. Margolis, Nucl. Phys. B11 (1969) 455
- Kö Sch 71 H.J. Körner and J.P. Schiffer, Phys. Rev. L. 27 (1971) 1457
- Leiss 58 J.E. Leiss and R.A. Schrack, Rev. Mod. Phys. 30 (1958) 456
- Lo Wi 76 R.J. Lombard and C. Wilkin, Contribution to the second Conference "Radial Shape of Nuclei", Cracow 1976, Lett. Nuov. Cim. 13 (1975) 463
- Leo 73 R. Leonardi, Phys. L. 43B (1973) 455
- Le Re 72 G.M. Lerner and E.F. Redish, Nucl. Phys. A193 (1972) 565
- Lern 72 G.M. Lerner, J.C. Hiebert, L.L. Rutledge, Jr. and A.M. Bernstein, Phys. Rev. C6 (1972) 1254
- Lern 75 G.M. Lerner, J.C. Hiebert, L.L. Rutledge, Jr., C. Papanicolas and A.M. Bernstein, Phys. Rev. C12 (1975) 778
- Les 72 P.M.S. Lesser, D. Cline, P. Goode and R.N. Horoshko, Nucl. Phys. A190 (1972) 597
- Le Se 74 M. Leon and R. Seki, Nucl. Phys. B74 (1974) 68
- Lom 72 J.C. Lombardi, R.N. Boyd, R. Arking and A.B. Robbins, Nucl. Phys. A188 (1972) 103
- Mac 71 R.S. Mackintosh, Nucl. Phys. A169 (1971) 398
- Mac 73 R.S. Mackintosh, Nucl. Phys. A198 (1972) 343
- Mac 76a R.S. Mackintosh, Z. Phys. A276 (1976) 25
- Mac 76b R.S. Mackintosh, Contribution to the Second Conference "Radial Shape of Nuclei", Cracow, Poland, June 22-25, 1976, - Oxford preprint 66/75
- Mac Ko 76 R.S. Mackintosh and A.M. Kobos, Oxford University Preprint 1976
- Mac Sw 75 R.S. Mackintosh and R. de Swiniarski, Phys. L. 57B (1975) 139
- Mac Ta 74 R.S. Mackintosh and J.L. Tassie, Nucl. Phys. A222 (1974) 187
- Mag 70 C.J. Maggiore, C.R. Gruhn, T.Y.T. Kuo and B.M. Preedom, Phys. L. 33B (1970) 571
- Mail 72 P. Mailandt, J.S. Lilley and G.W. Greenlees, Phys. Rev. L. 28 (1972) 1075
- Mail 73 P. Mailandt, J.S. Lilley and G.W. Greenlees, Phys. Rev. C8 (1973) 2189
- Mos 71 J.M. Moss, Y.D. Terrien, R.M. Lombard, C. Brassard, J.M. Loiseaux and F. Resmini, Phys. Rev. L. 26 (1971) 1488
- Na To 72 A. Nakada and Y. Torizuka, J. Phys. Soc. Japan 32 (1972) 1
- Neg 70 J.W. Negele, Phys. Rev. C1 (1970) 1260

- No Sch 69 J.A. Nolen, Jr. and J.P. Schiffer, Phys. L. 28B (1969) 396; Ann. Rev. of Nucl. Science 19 (1969) 471
- Ow Sa 70 L.W. Owen and G.R. Satchler, Phys. Rev. L. 25 (1970) 1720
- Pe Smi 73 D. Pelte and U. Smilansky, Proc. of the Minerva Symposium on Physics, Rehovot, April 2-5, 1973 - Lecture Notes in Physics 23, Springer-Verlag
- Ra Sp 71 G.M. Rawitcher and R.A. Spicuzza, Phys. L. 37B (1971) 221
- Re 71 H. Rebel, G.W. Schweimer, J. Specht, G. Schatz, R. Löhken, D. Habs, G. Hauser and H. Klewe-Nebenius, Phys. Rev. L. 26 (1971) 1190
- Re 72a H. Rebel, Nucl. Phys. A180 (1972) 332
- Re 72b H. Rebel, G.W. Schweimer, G. Schatz, J. Specht, R. Löhken, G. Hauser, D. Habs and H. Klewe-Nebenius, Nucl. Phys. A182 (1972) 145
- Re 74a H. Rebel, G. Hauser, G.W. Schweimer, G. Nowicki, W. Wiesner and D. Hartmann, Nucl. Phys. A218 (1974) 13
- Re 74b H. Rebel, G.W. Schweimer, D. Habs and H.J. Gils, Nucl. Phys. A225 (1974) 457
- Re 74c H. Rebel, Lectures given at the Int. Summer School of Nucl. Phys. Predeal, Romania, Sept. 1974, KFK-Report 2065 (1974)
- Re 76 H. Rebel, Z. Phys. A277 (1976) 35
- Re Ge 76 H. Rebel and H.V. v. Geramb, to be published, H. Rebel, KFK-Report 2247 (1976)
- Re Ha 73 H. Rebel and D. Habs, Phys. Rev. C8 (1973) 1391
- Re Sch 73 H. Rebel and G.W. Schweimer, Z. Phys. 262 (1973) 59
- Rho Ja 76 M. Rhoades-Brown and D.F. Jackson, Contribution to the Conference "Radial Shape of Nuclei", Cracow, Poland, June 22-25, 1976
- Rob 71 B.C. Robertson, J.T. Sample, D.R. Goosman, K. Nagatani and K.W. Jones, Phys. Rev. C4 (1971) 2176
- Ru Hi 76 L.L. Rutledge, Jr. and J.C. Hiebert, Phys. Rev. C13 (1976) 1072
- Sat 72 G.R. Satchler, J. Math. Phys. 13 (1972) 1118
- Sa Wi 74 J. Saudinos and C. Wilkin, Ann. Rev. of Nucl. Sci. 24 (1974) 341
- Schra 62 R.A. Schrack, J.L. Leiss and S. Penner, Phys. Rev. 127 (1962) 1772
- Si 75 P.P. Singh, P. Schwandt and G.C. Yang, Phys. L. 59B (1975) 113
- Sic 73 I. Sick, Phys. L. 44B (1973) 62, - Nucl. Phys. A218 (1974) 509
- Sin 75 B. Sinha, Phys. L. C (Phys. Reports) 20 (1975) 1
- Sl Mc 68 D. Slania and H. McManus, Nucl. Phys. A116 (1968) 271
- Swi 69 R. de Swiniarski, C. Glashausser, D.L. Hendrie, J. Sherman, A.D. Bacher and E.A. Mc Clatchie, Phys. Rev. L. 23 (1969) 317
- Swi 74 R. de Swiniarski, G. Bagieu, A.J. Cole, P. Gaillard, A. Guichard, J.Y. Grossiord, M. Gusakow, J.R. Pizzi, Journ. Phys. L. 35 (1974) L-26
- Swi 76 R. de Swiniarski, Contribution to the second Conference "Radial Shape of Nuclei", Cracow, 1976
- Sum 74 W.A. Summer, Ph.D. Thesis, University of Washington, 1974
- Tab 75 S.L. Tabor, B.A. Watson and S.S. Hanna, Phys. Rev. C11 (1975) 198

- Tab 76 S.L. Tabor, B.A. Watson and S.S. Hanna, Contrib. to the Conference "Radial Shape of Nuclei", Cracow, Poland, June 22-25, 1976
- Tat 72 B. Tatischeff, J. Brissaud and L. Bimbot, Phys. Rev. C5 (1972) 234
- Thir 74 J. Thirion, Proceed. of the Int. School of Nucl. Phys. Erice, 22. Sept. - 1. Oct., 1974, ed. H. Schopper, North-Holland 1975
- Th 73 G.L. Thomas, B.C. Sinha and F. Duggan, Nucl. Phys. A203 (1973) 305
- Th Sin 71 G.L. Thomas and B.C. Sinha, Phys. Rev. L. 26 (1971) 325
- Var Do 73 J.P. Vary and C.B. Dover, Phys. Rev. L. 31 (1973) 1510
- Wag 73 H. Wagner, A. Hofmann and F. Vogler, Phys. L. 47B (1973) 497
- Wat 53 K.M. Watson, Phys. Rev. 89 (1953) 291, - N.C. Francis and K.M. Watson, Phys. Rev. 92 (1953) 291
- Yar 76 Y. Yariv, T. Ledergerber and H.C. Pauli, Report MPH H-1976-V8